ФИЗИКА ЭЛЕМЕНТАРНЫХ ЧАСТИЦ И АТОМНОГО ЯДРА
2002. Т. 33. ВЫП. 2

УДК 539.17.17

EXPERIMENTAL STUDY OF COLLECTIVE FLOW PHENOMENA IN HIGH ENERGY NUCLEUS–NUCLEUS COLLISIONS

L. Chkhaidze, T. Djobava[*], *L. Kharkhelauri*

High Energy Physics Institute, Tbilisi State University, University St. 9, 380086 Tbilisi, Georgia

[*]e-mail: djobava@sun20.hepi.edu.ge or Tamar.Djobava@cern.ch

ФИЗИКА ЭЛЕМЕНТАРНЫХ ЧАСТИЦ И АТОМНОГО ЯДРА
2002. Т. 33. ВЫП. 2

УДК 539.17.17

EXPERIMENTAL STUDY OF COLLECTIVE FLOW PHENOMENA IN HIGH ENERGY NUCLEUS–NUCLEUS COLLISIONS

L. Chkhaidze, T. Djobava[*], *L. Kharkhelauri*

High Energy Physics Institute, Tbilisi State University, University St. 9, 380086 Tbilisi, Georgia

The results of experimental study of collective flow phenomena, such as the sideward and elliptic flow of nuclear matter, discovered during the last 10–15 years in high energy nucleus–nucleus collisions, are presented. In the review the results of the SKM-200-GIBS collaboration of JINR are presented and they are compared with the findings of different experiments of BEVALAC, GSI/SIS, AGS, and CERN/SPS. Different methods, proposed for the study of the flow effects in relativistic nuclear collisions, such as the directed transverse momentum analysis technique developed by Danielewicz and Odyniec and the method of the Fourier expansion of azimuthal distributions are described. The obtained signatures show the persistence of collective flow phenomena from the BEVALAC and GSI/SIS up to Dubna, AGS, RHIC and SPS energies. Studies based on transport models have indicated that the value for the transition energy $E_{\rm tr}$ depends on the nuclear equation of state (EOS) at high densities.

Представлены результаты экспериментального изучения коллективных потоковых явлений, таких как направленные и эллиптические потоки ядерной материи, обнаруженные за последние 10–15 лет в ядро-ядерных взаимодействиях при высоких энергиях. Результаты, полученные дубненской коллаборацией СКМ-200-ГИБС, сравниваются с данными других экспериментов на BEVALAC, GSI/SIS, AGS и CERN/SPS. Описаны разные методы изучения потоковых эффектов в релятивистских ядерных столкновениях, такие как метод анализа потоков в плоскости поперечного импульса и метод фурье-разложения азимутальных распределений. Полученные результаты показывают наличие (постоянство) коллективных потоковых явлений во всем диапазоне энергий от BEVALAC и GSI/SIS до Дубны, AGS и CERN/SPS. Исследования, проведенные на основе транспортных моделей, показывают, что величина энергии перехода $E_{\rm tr}$ зависит от уравнения состояния ядерной материи при больших плотностях.

1. COLLECTIVE NUCLEAR MATTER FLOW

One of the central goals of the experiments related with high-energy heavy ion collisions is a study of nuclear matter under extreme conditions of high density and temperature vastly different from that in normal nuclei. The most impressive results of high-energy heavy ion research so far are the new collective phenomena

[*]e-mail: djobava@sun20.hepi.edu.ge or Tamar.Djobava@cern.ch

discovered in these reactions. Collective processes are well established both experimentally and theoretically, such as different collective flow patterns. A collective flow is a motion characterized by space-momentum correlations of dynamic origin. In the energy range of 0.5–10 GeV/nucleon the nuclear matter is compressed and heated more than at lower beam energies.

The hot and compressed nuclear matter behaves like a compressible fluid, and fluid dynamical effects are observed in these reactions. A number of experiments have found that part of the compressional energy reappears in the form of collective flow effects of the matter. In the fluid dynamical approach the transverse collective flow is directly linked to the pressure $P(\rho, S)$ (depending on the density ρ and the entropy S) of the matter in the reaction zone: the generated collective transverse momentum $\mathbf{P}_x$ reflects the pressure (of the reaction zone) acting on a surface and over time [1].

$$\mathbf{P}_x = \int_t \int_A P(\rho, S)\, dAdt. \tag{1}$$

Here dA represents the surface element between the participant and spectator matters and the total pressure is the sum of the potential pressure and the kinetic pressure. The transverse collective flow depends directly on the equation of state (EOS), $P(\rho, S)$.

The collective flow had originally been predicted by nuclear shock wave models and ideal fluid dynamics [2–5].

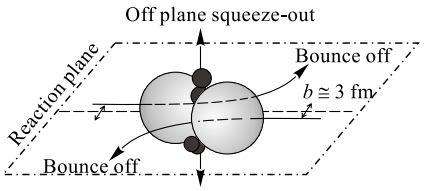

Fig. 1. Pictorial representation of the in-plane bounce-off and out-of-plane squeeze-out of participant matter predicted by fluid dynamics (figure from Ref. 9)

Two different signatures of the collective flow have been predicted (Fig. 1): a) the bounce-off [3] of compressed matter in the reaction plane (a sidewards deflection of the spectator fragments — «bounce-off», as well as the directed flow of nucleons from the overlap region between the colliding nuclei (participants) in the reaction plane — «side splash»), called the sideward (also often termed directed) flow; b) the squeeze-out [4] of the participant matter out of the reaction plane — the elliptic flow.

The reaction plane is the plane defined by the impact parameter $\mathbf{b}$ and the beam direction.

A strong dependence of these collective effects on the nuclear equation of state is predicted in Ref. 6. Due to its direct dependence on the EOS, $P(\rho, S)$, flow excitation functions can provide unique information about phase transitions: the formation of abnormal nuclear matter, e. g., yields a reduction of the collective flow [7, 8]. A directed flow excitation function as signature of the phase transition

into quark gluon plasma (QGP) has been proposed by several authors [7, 9–13].

The knowledge of EOS is of fundamental interest and is also essential for understanding astrophysical phenomena such as the supernova explosions, the properties of the core of compact stars (neutron stars), the evolution of the early Universe and the formation of elements in stellar nucleosynthesis.

A signature of the compression effects predicted by the calculations using a nontrivial EOS is collective flow of the nuclear matter in the expansion phase through the short range repulsion between the nucleons.

Collective effects lead to characteristic, azimuthally asymmetric sidewards emission of the reaction products. While the transverse flow in the reaction plane is influenced by the cold matter deflected by the overlap region of the colliding nuclei, the squeeze out is caused by the hot and compressed matter from the interaction region which preferentially escapes in the direction perpendicular to the reaction plane unhindered by the presence of the projectile and target spectators (Fig. 1).

Collective (the sideward and elliptic) flow has been discovered experimentally first at BEVALAC [14–16] for charged particles by the Plastic-Ball and Streamer Chamber collaborations [17] and at SATURNE (France) by the DIOGENE collaboration [18, 19]. It has been studied extensively at GSI by the FOPI [20, 21], LAND [22], TAPS [23] and KAOS [24] collaborations and by the EOS-TPC collaboration at LBNL (Berkeley) [25] and at MSU [26]. At AGS (Brookhaven National Laboratory — BNL) at the energy of 10.6 GeV/nucleon the collective flow has been discovered by the E877 collaboration [27, 28]. The EOS group has measured the flow excitation function for Au-Au at the AGS in the energy range between 2.0 and 8.0 GeV/nucleon [29]. Their data are corroborated by measurement of the E917 collaboration at 8 and 10.6 GeV/nucleon [30]. At JINR (Dubna) the sideward flow of spectator projectile fragments in Ne-Ag(Br) collisions at a momentum of 4.1 GeV/c/nucleon [31] and in Kr-Ag(Br) collisions at the energy of 0.95 GeV/nucleon [32] have been studied using emulsion detector. The Propane Buble Chamber collaboration at JINR studied the directed and elliptic flow of protons and negative pions in C-C collisions at a momentum of 4.2 GeV/c/nucleon [33]. Using emulsion detector at CERN/SPS, the first observations of the predicted directed transverse flow component [34] have been reported by the WA98 collaboration [35, 36] using the plastic-ball detector located at target rapidity for event plane reconstruction. Similar findings have also been reported by the NA49 collaboration, which due to their larger acceptance allows for a more detailed investigation [37]. At RHIC (Relativistic Heavy Ion Collider) of BNL the STAR collaboration recently reported first results on the elliptic flow of charged particles at midrapidity in Au-Au collisions at the energy of $\sqrt{S_{NN}} = 130$ GeV [38].

Many different methods were proposed for the study of flow effects in relativistic nuclear collisions, of which the most commonly used are the method

of directivity — the transverse momentum analysis technique developed by P. Danielewicz and G. Odyniec [39] — and the method of the sphericity (three-dimensional [40] or two-dimensional [41]) tensor. The transverse momentum analysis method of P. Danielewicz and G. Odyniec essentially relies on the determination of the reaction plane and then the transverse momenta of the emitted particles are projected (or rotated) to this reaction plane. This method has been used in our analysis and in the next section will be described in detail.

The method of the sphericity tensor [40] theoretically is straightforward to evaluate the real symmetric sphericity matrix in the c. m. frame:

$$S_{\alpha,\beta} = \sum_i \omega_i P_{i,\alpha} P_{i,\beta}, \qquad \alpha = \beta = x, y, z, \tag{2}$$

where i runs over all emitted charged particles and ω_i is a weight factor which may depend on the type of particle i. In the case of the «energy flow tensor» analysis $\omega_i = 1/2m_i$. The eigenvalues Q_i and the eigenvectors $\mathbf{e}_1$, $\mathbf{e}_2$, $\mathbf{e}_3$ of the tensor can be determined. If we normalize the sum of eigenvalues to unity so that $Q_3 \geq Q_2 \geq Q_1$, we can evaluate the commonly used quantities such as sphericity, jet angle, and aspect ratios. The tensor approximates the event shape by an ellipsoid whose orientation in space (jet angle $\Theta_{\text{c. m.}} = \arccos([\mathbf{e}_3]_z/e_3)$ and whose aspect ratios $R_1 = Q_3/Q_1$ and $R_2 = Q_2/Q_1$ can be calculated by diagonalizing the tensor. The vector $\mathbf{e}_3$ and the beam axis define the experimental reaction plane. After the reaction plane is determined, the other important task is to study the distribution of the flow angle Θ (the angle between $\mathbf{e}_3$ and the beam axis). The distribution of the flow angle is subject to very little experimental and statistical bias, so this was the first generally convincing evidence for the existence of collective flow.

A more general method to study transverse flow effects in relativistic nuclear collisions by Fourier analysis of the azimuthal distributions on an event-by-event basis in relatively narrow rapidity windows had been proposed by Demoulins et al. [19] and S. Voloshin and Y. Zhang [42]. This method includes as a part both directivity and two-dimensional sphericity methods in a natural way, clarifies their interrelation, and gives a clear physical meaning to the whole analysis. The distributions of Fourier coefficients provide information on the magnitude and type of flow. Fourier coefficients of different harmonics reflect the different types of anisotropy. The first harmonic coefficients then correspond to an overall shift of the distribution in the transverse plane; such flow is called the sideward (directed) flow. If one approximates the azimuthal distribution by an ellipse, then the second harmonic coefficient corresponds to an orientation of the ellipse perpendicular to the reaction plane, which is the case for the squeeze out flow and may be expected in the midrapidity window. A three-dimensional event shape can be obtained by correlating and combining the Fourier coefficients in different rapidity windows.

In this article the experimental results obtained using the transverse momentum analysis technique for protons and π^- mesons in C-Ne and C-Cu interactions at the energy of 3.7 GeV/nucleon at SKM-200-GIBS set-up of JINR (Dubna) are presented. The obtained signature shows the persistence of collective flow phenomena all the way from BEVALAC, GSI/SIS up to Dubna, AGS and SPS energies. Our results, obtained using the streamer chamber technique, provide quantitative information on the directed and elliptic flows and their dependence on beam energy and projectile/target mass, complementing the experimental data available from the BEVALAC, GSI/SIS, AGS and CERN/SPS.

2. METHODS OF FLOW STUDY IN RELATIVISTIC NUCLEUS–NUCLEUS COLLISIONS

2.1. Transverse Flow Analysis Method. The transverse momentum analysis method was introduced by P. Danielewicz and G. Odyniec [39]. It became a widely used sensitive method to detect the collective transverse flow. P. Danielewicz and G. Odyniec have proposed to present the collective effects as the distribution of average transverse momenta projected onto the reaction plane, as a function of rapidity. Transverse momentum is selected to avoid any possible effects due to nuclear transparency and corona [43] effects that would be manifested primarily in the longitudinal momenta.

The determination of the reaction plane is crucial in an experiment and it is possible only if the multiplicity, M, of the emitted particles is large and the major part of these particles is detected. The method involves two basic ideas:

1) to select the rapidity range and rapidity dependent waiting factors in the center-of-mass system, which provide the reaction plane closest to the real reaction plane, and

2) to remove trivial and spurious self-correlations from the projections.

The reaction plane is defined by the transverse vector $\mathbf{Q}$

$$\mathbf{Q} = \sum_{i=1}^{n} \omega_i \mathbf{P}_{\perp i}, \tag{3}$$

where i is a particle index and ω_i is a weight. Pions are not included. The reaction plane is the plane containing $\mathbf{Q}$ and the beam axis. The weight factor ω_i, depends on the rapidity of the emitted particle i, so that the central rapidity region, where the particle emission is azimuthally symmetric, is omitted, and the forward and backward rapidity regions get weight with opposite signs: ω_i is taken as 1 for $y_i > y_c$, -1 for $y_i < y_c$ and $\omega_i = 0$ for $-y_c < y_i < y_c$, where the cut-off rapidity y_c is usually chosen to be $y_c \approx 0.3 y_c^{\mathrm{beam}}$; y_i is the rapidity of particle i. This choice leads to the result that the forward and backward moving particles,

which are azimuthally anticorrelated if there is a transverse collective flow, will contribute equally to $\mathbf{Q}$.

To estimate the accuracy of the procedure each event has been divided in Ref. 39 randomly into two subevents (I and II) and the reaction plane vector in both half-events has been evaluated separately, getting $\mathbf{Q}_{\mathrm{I}}$ and $\mathbf{Q}_{\mathrm{II}}$. The two vectors should not be identical, but they should be close to each other if there was a real physical reaction plane in the underlying physical event. The azimuth angle difference between the two $\mathbf{Q}$ vectors is then $\Delta\phi$. Then the distributions of this $\Delta\phi$ have been plotted for the whole experimental sample. If there is a reaction plane and the weightening was lucky, one will get a distribution that peaks sharply around $\Delta\phi = 0$. An example of such a distribution has been obtained in Ref. 39. To verify that this result is not due to inefficiences in the streamer chamber acceptance, a similar one has been performed in [39] using Monte Carlo events generated by mixing particles from events within the same multiplicity range. The resulting distribition was completely flat.

The projection of the particle's (j's) transverse momentum to the reaction plane is

$$P'_{xj} = \mathbf{P}_{\perp j}\frac{\mathbf{Q}}{|\mathbf{Q}|}, \tag{4}$$

which can be expanded [44] as

$$P'_{xj} = \mathbf{P}_{\perp j}\frac{\sum\limits_{i=1}^{n}\omega_i\mathbf{P}_{\perp i}}{|\mathbf{Q}|} = \frac{\omega_j\mathbf{P}^2_{\perp j} + \sum\limits_{i\neq 1}\omega_i(\mathbf{P}_{\perp j}\mathbf{P}_{\perp i})}{|\mathbf{Q}|}. \tag{5}$$

If there would be no collective correlation

$$\langle P'_{xj}\rangle|_{y,y+\Delta y} = \frac{1}{\langle|\mathbf{Q}|\rangle}\left[\omega_j\langle\mathbf{P}^2_{\perp j}\rangle + \langle\sum_{i\neq 1}\omega_i(\mathbf{P}_{\perp j}\mathbf{P}_{\perp i})\rangle\right], \tag{6}$$

the expectation value in the second term would vanish $\langle\mathbf{P}_{\perp j}\mathbf{P}_{\perp i}\rangle = 0$ due to symmetry reasons, but the first term would not since $\mathbf{P}^2_{\perp j} \geq 0$. Thus this definition would yield a finite $\langle P'_{xj}\rangle|_{y,y+\Delta y}$ even if there are no real collective correlations in the sample. An example for this is shown in Fig. 2 taken from Ref. 39, where the real sample shows a clear anticorrelation between the forward and backward moving particles (Fig. 2, *a*). However in Ref. 39 the emitted particles from all events in the experimental sample have been taken and mixed randomly to form an artificial sample where the real physical correlations should be lost, the P_x plot still shows a clear azimuthal anticorrelation due to the self-correlation effect (Fig. 2, *b*).

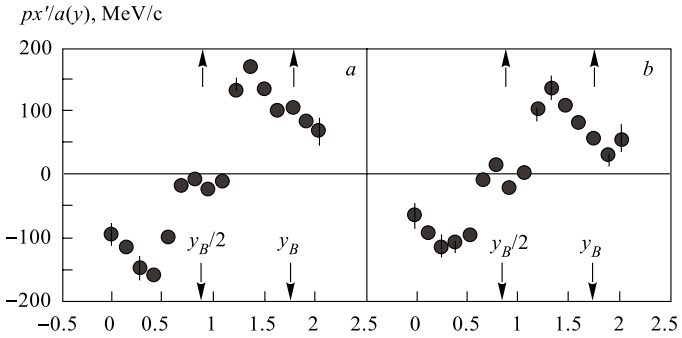

Fig. 2. Average in-plane transverse momentum per nucleon as a function of rapidity, from rotation of events to the reaction plane determined by $\mathbf{Q}$: *a*) for data — Ar-KCl at 1.8 GeV/nucleon; *b*) for Monte Carlo (figure taken from Ref. 39)

These self-correlations have been removed by removing the first term in expression (6). This can be done if we project each particle's transverse momentum to a reaction plane determined by all other particles

$$\mathbf{Q}_j = \sum_{i \neq j}^{n} \omega_i \mathbf{P}_{\perp i}. \tag{7}$$

Now the projection does not contain the self-correlation term

$$P'_{xj} = \frac{\sum\limits_{i \neq j} \omega_i (\mathbf{P}_{\perp j} \mathbf{P}_{\perp i})}{|\mathbf{Q}_j|}. \tag{8}$$

Thus P'_{xj} is nonzero only if real physical correlations exist. Figure 3 (taken from [39]) shows, that after removing the self-correlation from $\mathbf{P}_{\perp j}\mathbf{Q}$, the real sample still shows the azimuthal anticorrelation (Fig. 3, *a*), while the artificial sample shows no effect (Fig. 3, *b*).

The quantity P'_x underestimates the transverse momentum because the vector $\mathbf{Q}_j$ fluctuates around the real reaction plane by some azimuthal dispersion angle $\Delta\phi$. If one would know this real reaction plane, one could estimate the value of P_x projected to the real plane as:

$$\langle P_x \rangle = \langle P'_x \rangle / \langle \cos\, \Delta\phi \rangle. \tag{9}$$

In experiments $\Delta\phi$ is approximated by the width of the distribution of the azimuthal angle difference between the two reaction planes evaluated from each event in the sample.

It is important to understand that the deviation of $\mathbf{Q}_j$ from the real reaction plane is not caused only by the experimental resolution, it is due to the thermal

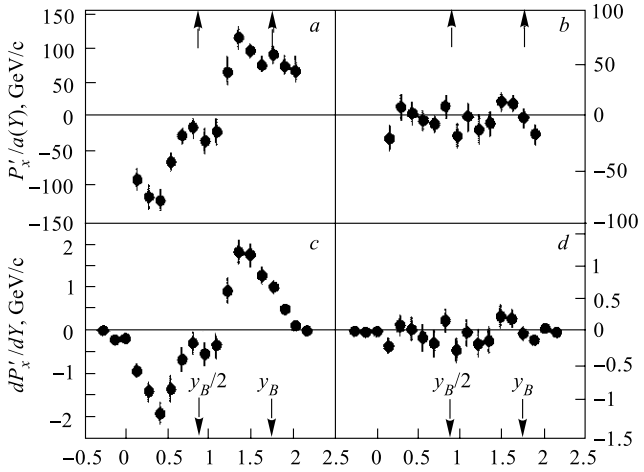

Fig. 3. *a, b*) Average momentum per nucleon in the estimated reaction plane $\langle P'_x/a\rangle(Y)$, upon removal of finite-multiplicity distortions, for data and Monte Carlo events, respectively. *c, d*) Differential, per unit rapidity, transverse momentum deposition in the estimated reaction plane in terms of nuclear charges $\langle dP'_x/dY\rangle$, for data and Monte Carlo events, respectively. Left-hand scales in (*a*) and (*c*) yield respective estimated average momenta per nucleon $\langle P_x/a\rangle(Y)$, and deposition $\langle dP_x/dY\rangle$, in the true reaction plane (figure taken from Ref. 39)

effects: the thermal energy leads to the emission of particles having a randomly oriented momentum, superimposed to the flow momentum. If the thermal momentum is small relative to the flow momentum, the final direction of the particles remains close to that of the reaction plane and Eq. (3) will lead to a good location of the reaction plane. In the opposite case, the influence of the flow momentum on the direction of the particle is washed out by the large thermal momentum. Even with an ideal detector which detects all particles with perfect angular, mass and energy resolution, $\Delta\phi$ can be large.

A practical definition, the «flow» F, was introduced by the Plastic-Ball team later [15] to measure the transverse momentum transfer:

$$F = \left.\frac{\partial[P_x]}{\partial Y}\right|_{y_{\mathrm{c.m.s}=0}} . \tag{10}$$

This quantity was subject of less experimental bias than the maximum of P_x, and it enabled to compare different reactions and results of different experimental set-ups to each other.

2.2. The Method of Fourier Expansion of Azimuthal Particle Distributions. The azimuthal distributions of particles can be constructed from different quan-

tities such as transverse momentum P_t, multiplicity, or transverse energy E_t in relatively narrow (pseudo)-rapidity windows. To get more details of the event shapes one would like to divide the whole (pseudo)-rapidity acceptance into more windows. The limitation is that there should be a sufficient number of particles in each window to keep the fluctuations under control.

Within a rapidity window, flow causes anisotropic distributions of track azimuths ϕ relative to the reaction plane. To describe the anisotropy in particle production, by Demoulins et al. [19] and Valoshin and Zhang, [42] there has been introduced the method of the Fourier expansion of the azimuthal distributions, where the anisotropic flow signal is represented by the Fourier coefficients v_n — the amplitudes of different harmonics:

$$\frac{d^2N}{dP_t d\phi} = \frac{dN}{dP_t}\left[1 + \sum_{n=1}^{n=\infty} 2v_n(y, P_t)\cos(n\phi)\right], \tag{11}$$

where $v_n = \langle\cos(n\phi)\rangle$.

In actual experiment, the reaction plane is not known exactly and is reconstructed event by event from the reaction products. The reconstructed plane differs from the true reaction plane by an error $\Delta\phi$, which varies from one event to the other. Thus, the measured azimuthal angle ψ is related to the true azimuthal angle ϕ by $\psi = \phi - \Delta\phi$ (see Fig. 4, taken from Ref. 45). Averaging over many events, assuming that ϕ and $\Delta\phi$ are statistically independent, one obtains the following relation between the measured and true Fourier coefficients [19, 28, 41, 45]:

$$\langle\cos(n\psi)\rangle = \langle\cos(n\phi)\rangle\langle\cos(n\Delta\phi)\rangle, \tag{12}$$

$$v_n' = v_n\langle\cos(n\Delta\phi)\rangle.$$

From Eq. (12), one can reconstruct the true distribution once the correction factor $\langle\cos(n\Delta\phi)\rangle$ is known. Ollitrault proposed a general method of reconstructing the Fourier coefficients of the true azimuthal distributions from the measured ones by means of analytical formulae [41, 45]. In this method [45] as in Ref. 39 for estimation of the accuracy of the reaction plane determination, each event is divided randomly into two subevents containing half of the particles each, and vector $\mathbf{Q}$ is constructed for two subevents [39]

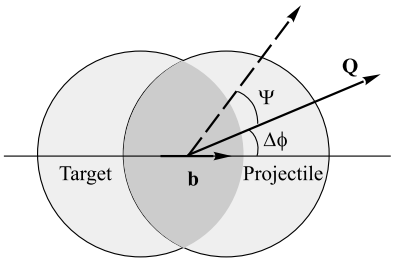

Fig. 4. Schematic picture of a semicentral nucleus–nucleus collision viewed in the transverse plane (the beam axis is orthogonal to the figure). $\mathbf{b}$ is the impact parameter oriented from the target to the projectile and $\mathbf{Q}$ is the vector defined by Eq. (3). A particle is emitted along the dashed arrow. Its azimuthal angle measured with respect to $\mathbf{Q}$ is ψ, while the «true» azimuthal angle is $\psi + \Delta\phi$ (figure taken from Ref. 45)

(see Sect. 2.1). One thus obtains two vectors $\mathbf{Q}_{\mathrm{I}}$ and $\mathbf{Q}_{\mathrm{II}}$. It is assumed, that the fluctuations of $\mathbf{Q}$ (also $\mathbf{Q}_{\mathrm{I}}$ and $\mathbf{Q}_{\mathrm{II}}$, respectively) around its average value $\langle Q\rangle$ ($\langle Q_{\mathrm{I}}\rangle$ and $\langle Q_{\mathrm{II}}\rangle$, respectively) are Gaussian. However, since each subevent contains only $N/2$ particles (N — number of particles entering the definition of the vector $\mathbf{Q}$), the corresponding average value and fluctuations must be scaled: $\langle Q_{\mathrm{I}}\rangle = \langle Q_{\mathrm{II}}\rangle = \langle Q\rangle/2$, $\sigma_{\mathrm{I}} = \sigma_{\mathrm{II}} = \sigma/\sqrt{2}$. The distribution of the relative angle $\Delta\phi_R = |\Delta\phi_{\mathrm{I}} - \Delta\phi_{\mathrm{II}}|$ can be calculated analytically [41]. For $\langle\cos(\Delta\phi_R)\rangle$ one can obtain [41, 45]:

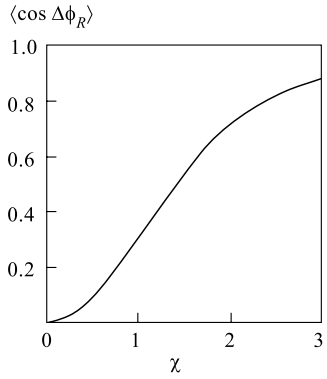

Fig. 5. Variation of $\langle\cos(\Delta\phi_R)\rangle$ with χ, given by Eq. (13) (figure taken from Ref. 45)

$$\langle\cos(\Delta\phi_R)\rangle = \langle\cos(\Delta\phi_{\mathrm{I}})\rangle\langle\cos(\Delta\phi_{\mathrm{II}})\rangle = \\ = \frac{\pi}{8}\chi^2 \mathrm{e}^{-\chi^2/2}\left[I_0\Big(\frac{\chi^2}{4}\Big) + I_1\Big(\frac{\chi^2}{4}\Big)\right]^2, \tag{13}$$

where I_0 and I_1 are the modified Bessel functions. The dimensionless parameter $\chi = \langle Q\rangle/\sigma$ is introduced to measure the accuracy of the reaction plane determination in Ref. 45. The χ scales simply with the multiplicity like $\sqrt{N}$. It has a simple physical interpretation, being the ratio of the average value of the flow vector $\mathbf{Q}$ to the typical statistical fluctuation σ. If one extracts from Eq. (13) the crucial parameter χ (see Fig. 5, taken from Ref. 45), then the correction factor $\langle\cos(n\Delta\phi)\rangle$ can be calculated via the following formula [45]:

$$\langle\cos(n\Delta\phi)\rangle = \frac{\sqrt{\pi}}{2}\chi^2 \mathrm{e}^{-\chi^2/2}\left[I_{\frac{n-1}{2}}\Big(\frac{\chi^2}{2}\Big) + I_{\frac{n+1}{2}}\Big((\chi^2)/2\Big)\right], \tag{14}$$

where I_k is the modified Bessel function of order k. In the limit $\chi \gg 1$ the correction factor is given by [45]:

$$\langle\cos(n\Delta\phi)\rangle \;\simeq\; \exp(-n^2/4\chi^2) \tag{15}$$

and in the limit $\chi \ll 1$ [45]

$$\langle\cos(n\Delta\phi)\rangle \;\simeq\; \frac{\sqrt{\pi}}{2^n\Gamma\left(\dfrac{n+1}{2}\right)}\chi^n, \tag{16}$$

where Γ is the Euler function. The variations of the first coefficients with χ are displayed in Fig. 6 (taken from Ref. 45). The value of $\cos(n\delta\phi)$ decreases with increasing n, and becomes vanishingly small for $n \gg \chi$.

The anisotropic directed collective flow has been studied most commonly by analyzing the average transverse momentum per nucleon in the reaction plane as a function of rapidity Y [39].

$$\langle P_x\rangle(Y) = \frac{1}{dN/dY}\int P_t \frac{d^2N}{dP_t dY} \times \times\langle\cos(\phi)(Y,P_t)\rangle dP_t, \quad (17)$$

ϕ is the azimuthal angle of particles with respect to the reaction plane and

$$\langle\cos\,\phi\rangle(Y,P_t) \equiv \equiv \left(\frac{dN}{dP_t}\right)^{-1}\int \cos(\phi)\frac{d^2N}{dP_t d\phi}d\phi. \quad (18)$$

A nonvanishing $\langle\cos\,\phi\rangle(Y,P_t)$ indicates the existence of an azimuthally anisotropic transverse flow at the rapidity Y and transverse momentum P_t. Adopting the Fourier expansion (11) one finds that

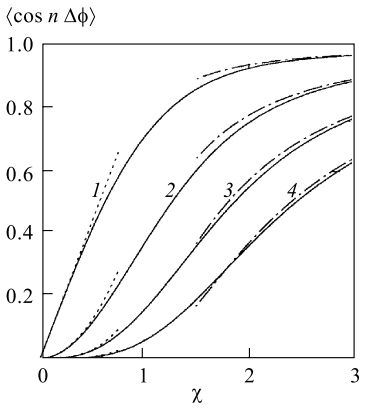

Fig. 6. Solid lines — variation of $\langle\cos(n\Delta\phi)\rangle$ with the parameter χ, calculated from Eq. (14). The curves are labeled by the value of n. The dotted and dash-dotted curves are the asymptotic form given respectively by Eqs. (16) and (15) (figure taken from Ref. 45)

$$\langle\cos(\phi)\rangle(Y,P_t) = v_1(Y,P_t) \quad (19)$$

is the strength of the azimuthal angle distribution to the first order. Thus the first Fourier coefficient, v_1 reflects the azimuthal angular part of the sideward flow correlation and is related to the $\langle P_x\rangle$ sideward flow observable according to Ref. 42

$$v_1 = \left\langle\frac{P_x}{P_t}\right\rangle. \quad (20)$$

If one approximates the azimuthal distribution by an ellipse, then the second Fourier coefficient v_2 is proportional to the magnitude of the eccentricity and reflects (describes) elliptic flow, which is expected in the midrapidity window. $v_2 > 0$ indicates in-plane enhancement; $v_2 < 0$, the squeeze-out perpendicular to the reaction plane and $v_2 = 0$ shows an isotropic distribution in the transverse plane. The v_2 is related [42] to the x and y components of particle transverse momentum, i. e.,

$$v_2 = \left\langle\left(\frac{P_x}{P_t}\right)^2 - \left(\frac{P_y}{P_t}\right)^2\right\rangle, \quad (21)$$

where the average is taken over all particles of a given kind in all events [42].

3. DIRECTED FLOW OF PROTONS AND π^- MESONS

3.1. Protons. It has been demonstrated in Ref. 13 by Hung and Shuryak, that the hydrodynamic evolution of excited nuclear matter does change dramatically as the initial energy density goes through the «softest point» (where the pressure to energy density ratio reaches its minimum). The «softest point» of the equation of state is resulted in a possible formation of a long-lived fireball in nuclear collisions [13, 46] (the «softest point» effect) which may serve as a signal of the QCD deconfinement phase transition [13, 46]. The directed nucleon flow characterizing the nuclear matter bounce-off in respect of the reaction plane is an example of the observable [46] to be used to observe the «softest point» effect. In Ref. 47 assuming a full stopping, a deep minimum in the excitation function for the directed flow has been predicted at $E_{\rm lab} \approx 5$ GeV/nucleon. Hung and Shuryak [13] assumed that only half an energy is attainable for the hydrodynamic stage that shifts the expected energy to a noticebly higher value $E_{\rm lab} \approx$ 30 GeV/nucleon. The statistical mixed phase (MP) model [46], in which the hypothesis on coexistence of hadrons and unbound quarks/gluons in nuclear matter has been realized, predicts that the «softest point» is located at energy density of $\varepsilon_{\rm SP} \approx 0.5$ GeV/fm^3 and might by observed at energies below 10 GeV/nucleon. In view of the above mentioned, it is clear the importance of observation of flow effects in the energy region of 3–10 GeV/nucleon. The flow effects at energy of $E_{\rm lab} \approx 4$ GeV/nucleon have been studied by SKM-GIBS collaboration.

The data were obtained on the SKM-200-GIBS set-up at JINR. SKM-GIBS consists of a 2 m streamer chamber, placed in a magnetic field of 0.8 T, and a triggering system. The streamer chamber was exposed to the beam of C and Mg nuclei accelerated in the synchrophasotron up to the energy of 3.7 GeV/nucleon. The thickness of the solid targets in the shape of a thin discs was 0.2 g/cm^2 for Cu and 1.56 g/cm^2 for Mg. Neon gas filling the chamber also served as a nuclear target. The triggering system allowed the selection of «inelastic» and «central» collisions. The «central» trigger was selecting events with no charged projectile spectator fragments (with $P/Z > 3$ GeV/c) within a cone of half-angle $\Theta_{\rm ch} = 2.4^\circ$ or 2.9°. The trigger efficiency for events with a single charged particle in the cone was 99 %. The ratio $\sigma_{\rm cent}/\sigma_{\rm inel}$ that characterizes the centrality of selected events is $(9 \pm 1)\,\%$ for C-Ne and $(21 \pm 3)\,\%$ for C-Cu. Based on Dubna Cascade Model [48] simulations, it is estimated that selected events correspond to a mean impact parameter $\langle b \rangle = 2.15$ fm for C-Ne and $\langle b \rangle = 3.25$ for C-Cu collisions. According to the quark gluon string model (QGSM) [11] simulations the selected events correspond (see below) to $\langle b \rangle = 2.20$ fm for C-Ne and $\langle b \rangle = 2.75$ fm for C-Cu, respectively. Average measurement errors of the momentum and production angles are: for protons $\langle \Delta P/P \rangle = (8 \div 10)\,\%$, $\Delta\Theta = 1 \div 2^\circ$; for pions $\langle \Delta P/P \rangle = 5\,\%$, $\Delta\Theta = 0.5^\circ$ in C-Ne and C-Cu collisions and $\langle \Delta P/P \rangle = 1.5\,\%$, $\Delta\Theta = 0.3^\circ$ for pions in Mg-Mg interactions.

The data have been analyzed event by event [49] using the transverse momentum technique of Danielewicz and Odyniec [39].

The reaction plane (plane containing **Q** and the beam axis) has been defined for the participant protons, i. e., protons which are not fragments of the projectile ($P/Z > 3$ GeV/c, $\Theta < 4^\circ$) and target ($P/Z < 0.2$ GeV/c). They represent the protons participating in the collision. The number of events and the average multiplicities of analyzed protons $\langle N_p \rangle$ in C-Ne and C-Cu interactions are listed in Table 1.

Table 1. **The number of experimental and QGSM simulated events, the average multiplicity of participant protons $\langle N_p \rangle$, the mean rapidity $\langle Y \rangle$, the correction factor $k_{\rm corr}$, the flow F and the average transverse momentum per nucleon in the reaction plane in the forward hemisphere of the c. m. system $\langle P_x \rangle_{y>0}$**

	C-Ne	C-Cu
Number of exper. events	723	663
Number of generated events, b not fixed	2925	3194
Number of generated events, b fixed	$b = 2.20$ fm 8400	$b = 2.75$ fm 9327
$\langle N_p \rangle_{\rm exp}$	12.4 ± 0.5	19.5 ± 0.6
$\langle N_p \rangle_{\rm mod}$, not fixed b	11.5 ± 0.2	21.7 ± 0.3
$\langle N_p \rangle_{\rm mod}$, fixed b	12.0 ± 0.2	22.6 ± 0.3
$\langle Y \rangle_{\rm exp}$	1.07 ± 0.07	0.71 ± 0.08
$\langle Y \rangle_{\rm mod}$, not fixed b	1.03 ± 0.03	0.64 ± 0.05
$\langle Y \rangle_{\rm mod}$, fixed b	1.05 ± 0.03	0.62 ± 0.05
$k_{\rm corr} = 1/\langle \cos \phi_{12} \rangle$ by method [39]	1.27 ± 0.08	1.31 ± 0.04
$k_{\rm corr}$ by method [51]	1.42 ± 0.06	1.39 ± 0.04
$F_{\rm exp}$ (lab.), MeV/c (for protons, not corrected by $k_{\rm corr}$)	109 ± 10	161 ± 15
$F_{\rm exp}$ (lab.), MeV/c (for protons, corrected by $k_{\rm corr}$ [39])	134 ± 12	198 ± 13
$F_{\rm exp}$ (lab.), MeV/c (for π^- mesons, corrected by $k_{\rm corr}$ [39])	29 ± 5	–47 ± 6
$F_{\rm QGSM}$, MeV/c, not fixed $\tilde{b}$ (for protons)	92 ± 8	164 ± 14
$F_{\rm QGSM}$, MeV/c, fixed b (for protons)	95 ± 9	153 ± 13
$\langle P'_x \rangle_{y>0}$, MeV/c	74 ± 8	114 ± 12
$\langle P_x \rangle_{y>0}$ multiplied on $k_{\rm corr}$ by method [39]	97 ± 11	145 ± 18

For the event-by-event analysis it is necessary to perform an identification of π^+ mesons, the admixture of which amongst the charged positive particles is about $(25 \div 27)\,\%$. The statistical method has been used for identification of π^+ mesons. The main assumption is based on the similarity of spectra of π^- and

π^+ mesons (n_π, P_T, P_L). The two-dimentional — transverse and longitudinal — momentum distribution (P_T, P_L) has been used for identification of π^+ mesons. The whole plane is divided into 7 zones. For example for C-Ne collisions:
1) $P_L > 2.5$ GeV/c or $P_T > 0.9$ GeV/c;
2) $0 \leq P_L \leq 1.4$ GeV/c and $P_T \leq 0.7$ GeV/c — PMAX;
3) $0 \leq P_L \leq 1.4$ GeV/c and $P_T > 0.7$ GeV/c;
4) $P_L > 1.4$ GeV/c (< 2.5 GeV/c);
5) $-0.2 \leq P_L \leq 0$ GeV/c and $P_T \leq 0.3$ GeV/c;
6) $-0.2 \leq P_L \leq 0$ GeV/c and $P_T > 0.3$ GeV/c;
7) $P_L < -0.2$ GeV/c.
The zone 2 of maximal overlap — PMAX — in its turn is divided into $7 \times 7 = 49$ cells. The probability of hitting each zone and respectively the cell by π^- mesons and charged positive particles is defined and the relative probability of hitting of π^- mesons is calculated as a result. The admixture of π^+ mesons in the zone 1 is negligible. The procedure of dividing the (P_T, P_L) plane into the cells allows one to simplify the mathematical algorithm and improves the accuracy of the identification. In Fig. 7 the division of the (P_T, P_L) plane is presented for C-Ne collisions. It was assumed, that π^+ and π^- mesons hit the given cell with equal probability (the equal probability densities for π^+ and π^- were assumed).

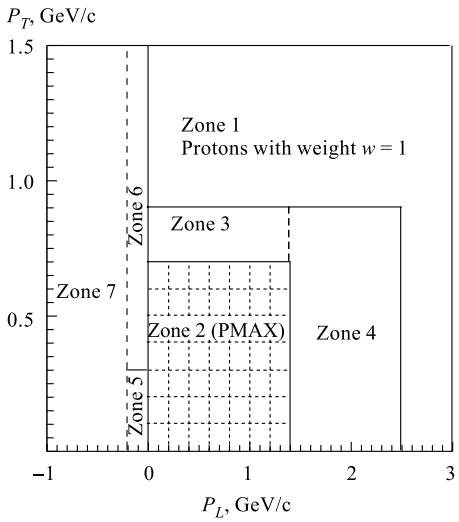

Fig. 7. Two-dimentional (P_T, P_L) plot in C-Ne collisions for the identificaton of protons and π^+ mesons

The identification in fact is equal to summing of hitting probabilities into each cell and when the sum reaches the critical value, the particle is considered as π^+ meson. The rest of particles are assumed to be protons. For each proton and π^+ meson the sign is recorded on DST (data summary tape), which indicates to which zone of (P_T, P_L) plane the given particle belongs and what is the probability. Particles with $P_T > 0.9$ GeV/c or $P_L > 2.5$ GeV/c are unambiguous protons with probability equal to 1.

After identification of π^+ mesons in the event, the difference of π^+ and π^- mesons Δn is determined. If $|\Delta n| > 2$, in the region PMAX the identification $\pi^+ \leftrightarrow P$ is interchanged and for that reason particles with smaller probability are chosen. If the condition of approachement of multiplicities is not fulfiled, then in

this case into the «head» information of the event such a sign is recorded, which allows one to exclude the given event from the further analysis.

After performed identification the admixture of π^+ mesons amongst the protons is not exceeding $(5 \div 7)\,\%$.

As we study an asymmetric pair of nuclei, we chose to bypass the difficulties associated with the centre-of-mass determination and carried out the analysis in the laboratory frame. The original weight ω_i has been replaced by the continuous function $\omega_i = y_i - \langle y \rangle$ as in [50], where $\langle y \rangle$ is the average rapidity, calculated for each event over all the participant protons. The value of the weight ω_i should be chosen to minimize the fluctuations of $\mathbf{Q}_j$ from the true reaction plane.

As is known [39, 50, 51], the estimated reaction plane differs from the true one, in particular, due to the finite multiplicity. The component P_x in the true reaction plane is systematically larger than the component P'_x in the estimated plane (see formula (9)), where ϕ is the angle between the estimated and true planes. The correction factor $k_{\rm corr} = 1/\langle \cos \Delta\phi \rangle$ is subject to a large uncertainty, especially for low multiplicity. According to [39], for the definition of $\langle \cos \Delta\phi \rangle$ we divided randomly each event into two equal subevents, constructed vectors $\mathbf{Q}_1$ and $\mathbf{Q}_2$ and estimated azimuthal angle ϕ_{12} between these two vectors. $\langle \cos \Delta\phi \rangle = \langle \cos \phi_{12} \rangle$. The data did not allow one to perform the analysis for different multiplicity intervals, therefore we defined the correction factors $k_{\rm corr}$, averaged over all the multiplicities. The values of $k_{\rm corr}$ are listed in Table 1. For the estimation of $\langle \cos \Delta\phi \rangle$ the alternative method [51] has been applied also, which does not require the division of each event into two subclasses.

$$\langle \cos \Delta\phi \rangle \approx \langle \omega P'_x \rangle [\langle W^2 - W \rangle / \langle Q^2 - \sum (\omega_i P_{\perp i})^2 \rangle]^{1/2}, \tag{22}$$

where $W = \sum |\omega_i|$. These two methods yield consistent results within the errors (Table 1).

Figure 8, *a, b* shows the dependence of the estimated $\langle P'_x(Y) \rangle$ on Y for protons in C-Ne and C-Cu collisions. The average transverse momentum $\langle P'_x(Y) \rangle$ is obtained [49] by averaging over all events in the corresponding intervals of rapidity. The data exhibit the typical S-shape behaviour which demonstrates the collective transverse momentum transfer between the forward and backward hemispheres. The directed flow is an odd function of the rapidity. It is therefore linear near midrapidity. Furthermore, a saturation is observed near projectile and target rapidities, resulting in a typical S shape [39].

From the mean transverse momentum distibutions one can extract two main observables sensitive to the EOS. One of them is the mean transverse momentum averaged for positive values of rapidity $\langle P_x \rangle_{y>0}$. A somehow equivalent observable is the transverse flow $F = \dfrac{d\langle P_x \rangle}{dY}$, i. e., the slope of the momentum distribution at midrapidity. It is the measure of the amount of collective transverse momentum transfer in the reaction, i. e., intensity of the nuclear interactions.

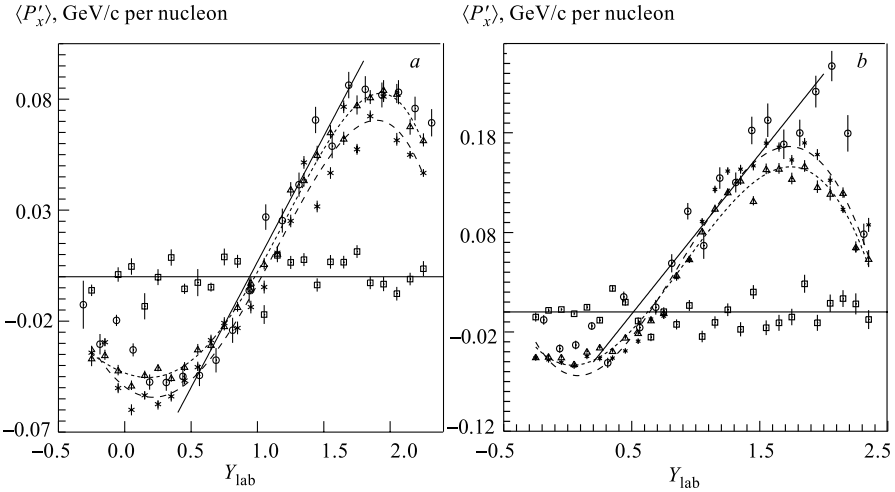

Fig. 8. The dependence of $\langle P'_x(Y)\rangle$ on $Y_{\rm lab}$ for protons in C-Ne (*a*) and C-Cu (*b*) collisions: $\circ$ — the experimental data; $\triangle$ — QGSM generated data for fixed $b = 2.20$ fm (*a*) and $b = 2.75$ fm (*b*); $*$ — QGSM generated data for not fixed $\tilde{b}$; $\square$ — events composed by randomly selected tracks from different QGSM events (within the same multiplicity range). The solid line is the result of the approximation of experimental data by sum of first- and third-order polynomial functions in the interval of Y — $0.4 \div 1.9$ (*a*) and $0.2 \div 2$ (*b*). The dashed curves for visual presentation of QGSM events (short dashes — for fixed b, long dashes — for not fixed $\tilde{b}$) — result of approximation by the 4th order polynomial function

Technically F is obtained by fitting the central part of the dependence of $\langle P'_x(Y)\rangle$ on Y with a sum of the first and third order polynomial functions. The coefficient of the first order term is the flow F. The fit was done for Y between $0.4 \div 1.9$ for C-Ne and $0.2 \div 2$ for C-Cu. The straight lines in Fig. 8, *a, b* show the results of this fit for the experimental data. The values of F are listed in Table 1. The value of measured flow F is normally less than the true value because $P'_x < P_x$. The obtained values of F can be considered as lower limits of the nuclear flow in C-Ne and C-Cu collisions. The influence of the admixture of ambiguously identified π^+ mesons on the results has been analyzed. The error in flow F includes the statistical and systematical errors.

In order to compare our experimental results with the ones obtained from the different experiments with various energies and masses, results for both C-Ne and C-Cu collisions have been presented in terms of the normalized rapidity in the laboratory system $Y/Y_{\rm proj}$, where $Y_{\rm proj} = 2.28$ is the projectile rapidity [52].

Figure 9 shows the dependence of $\langle P_x\rangle$ on the normalized rapidity $Y/Y_{\rm proj}$ in the laboratory system for protons in C-Ne and C-Cu collisions [52]. For protons

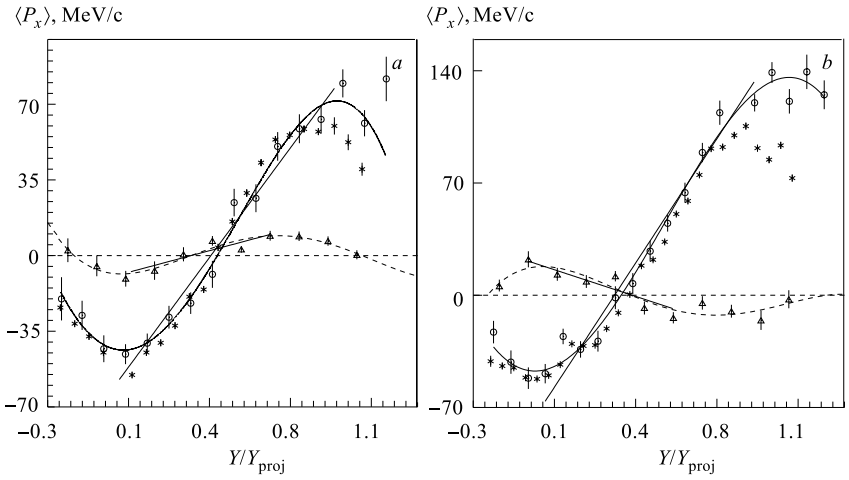

Fig. 9. The dependence of $\langle P_x \rangle$ on the normalized rapidity $Y/Y_{\rm proj}$ in the laboratory system in C-Ne (*a*) and C-Cu (*b*) collisions: $\circ$ — for protons; $\triangle$ — for π^- mesons; $*$ — the QGSM data for protons. The lines represent fits of experimental data in the intervals $0.01 \leq Y/Y_{\rm proj} \leq 0.90$ for protons and $0.04 \leq Y/Y_{\rm proj} \leq 0.70$ (*a*) and $-0.06 \leq Y/Y_{\rm proj} \leq 0.6$ (*b*) for π^- mesons. The curves show the 4th order polynomial fits

the data points are multiplied by the factor $k_{\rm corr}$ (by the method of Ref. 39) described above to correct for the deviation from the true reaction plane. The flow $F = d\langle P_x \rangle / d(Y/Y_{\rm proj})$. The fit was done for $Y/Y_{\rm proj}$ between $0.01 \div 0.90$. The straight lines in Fig. 9, *a, b* show the results of this fit. The values of F extracted from Fig. 9 are listed in Table 1. One can see from Table 1, that with the increase of the mass number of the target A_T the value of F increases. A similar tendency was observed at lower energies [15, 25, 51, 53–55].

An estimation of F from streamer chamber data on Ar-KCl at 0.8 and 1.2 GeV/nucleon gives value of 100 MeV/c in agreement with the Plastic-Ball data for Ca-Ca at the same energy. Comparing these findings with our result for C-Ne (see Table 1), one can conclude, that F increases systematically in the energy region of $0.8 \div 4$ GeV/nucleon. For the heavier system of Nb-Nb [55] the flow F increases from 135 MeV/c at 0.4 GeV/nucleon to 160 MeV/c at 1.05 GeV/nucleon.

The EOS collaboration has determined the nucleon (proton) flow for central Ni-Cu and Ni-Au collisions over an energy range of 0.4 to 1.97 GeV/nucleon [25]. The flow increases with energy, reaches a maximum and then gradually decreases at higher energies (Ni-Au: $F = 300$ MeV/c for 0.4 GeV/nucleon, $F = 400$ MeV/c for 0.6 GeV/nucleon, $F = 414$ MeV/c for 1.0 GeV/nucleon, $F = 240$ MeV/c for

1.97 GeV/nucleon; Ni-Cu: $F = 280$ MeV/c for 1.0 GeV/nucleon, $F = 260$ MeV/c for 1.5 GeV/nucleon, $F = 220$ MeV/c for 2.0 GeV/nucleon). Our result for the flow for lighter system (C-Cu) at higher energy ($E = 3.7$ GeV/nucleon) is smaller than the flow obtained by the EOS for Ni-Cu at 2 GeV/nucleon. The EOS collaboration has obtained the flow for protons in Au-Au collisions also at the energy of 1.15 GeV/nucleon, $F = 187$ MeV/c.

During several years the region between maximum BEVALAC/SIS energy ($\sim$ 2 GeV/nucleon) and maximum AGS energy (~ 14.7 GeV/nucleon) has been rather unexplored. Our results at a momentum of 4.5 GeV/c ($E = 3.7$ GeV/nucleon), presented here, were one of the first results for light nuclear systems in the region of 4 GeV/nucleon. More recently the Propane Buble Chamber collaboration of JINR has reported [33] the results on the study of the protons directed flow in C-C collisions at a momentum of 4.2 GeV/c/nucleon. It is found, that the protons exhibit pronounced directed flow and the value of flow at mid-rapidity ($0.7 < Y < 1.5$) $F = 144$ MeV/c. This result agrees with our flow for C-Ne collisions (Table 1). Recently the E895 collaboration [29] have reported about measurements of collective sideward flow for protons in semicentral Au-Au collisions at beam energies of 2.0, 4.0, 6.0 and 8.0 GeV/nucleon. The results have been presented in the form of in-plane transverse momentum $\langle P_x \rangle$ and the first Fourier coefficient of azimuthal anisotropy. These measurements indicate that sideward flow decreases smoothly over the 2.0 to 8.0 GeV/nucleon range ($F = 238 \pm 15$ for 2.0 GeV/nucleon, $F = 205 \pm 19$ for 4.0 GeV/nucleon, $F = 183 \pm 16$ for 6.0 GeV/nucleon, $F = 164 \pm 20$ for 8.0 GeV/nucleon). One can see that our results are corroborated by their measurements at 4.0 GeV/nucleon and also the measurements of E895 at 8.0 GeV/nucleon are consistent with the measurements of the E917 collaboration at 8.0 and 10.6 GeV/nucleon [30]. At AGS energy of 10.8 GeV/nucleon the flow has been discovered by the E877 collaboration for protons and pions in Au-Au collisions [27, 28] by measuring $dv_1/d\eta = d(\langle E_x \rangle / \langle E_T \rangle)/d\eta$ for different centrality bins, (η is pseudorapidity), where E_T is the transverse energy, $E_T = \sqrt{P_T^2 + m^2}$ and E_x is its projection on x direction (axis). In order to compare their results to data available from lower beam energies, $\langle P_x \rangle$ has been evaluated as a function of the rapidity and slope F. From the analysis a value of $F = 137$ MeV/c has been obtained.

The first evidence of directed flow at SPS/CERN was reported by the WA89 collaboration [35, 36], more recent measurements have been made by the NA49 [37] collaboration. The directed flow of protons has been studied in 158 GeV/nucleon Pb-Pb collisions. A directed flow analysis of the rapidity dependence of the average transverse momentum projected onto the reaction plane was presented for semicentral collisions. The value of $\langle P_x \rangle$ in the fragmentation region in NA49 at SPS/CERN was at least three times smaller than at AGS. The directed flow at SPS seems to be concentrated in the fragmentation regions, and almost absent in the central rapidity region: the rapidity dependence does not follow an S-shaped

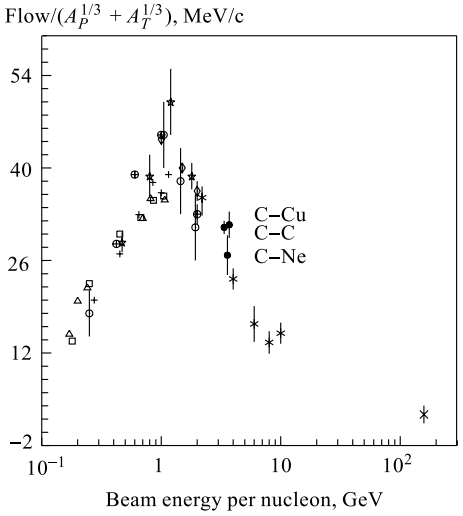

Fig. 10. Scaled flow values versus beam energy per nucleon, for different projectile/target systems: □ — Nb-Nb Plastic Ball; ⊕ — Ni-Au EOS; △ — Au-Au Plastic Ball; ○ — Ni-Ni FOPI; ◇ — Ni-Cu EOS; + — Au-Au EOS; ⋆ — Ar-Pb Streamer Chamber, the value at $E = 1.08$ A GeV represents Ar-KCl Streamer Chamber; • — C-Ne, C-Cu (our result); C-C (Propane collaboration); ∗ — Au-Au E895, the value at $E = 10$ A GeV represents Au-Au from E877; × — Pb-Pb NA49. To improve the distinction between data points at the same beam energy, some of the beam energy values have been shifted

curve (deviations from this shape are already seen at AGS by E917 [30]) and the flow parameter, obtained as the slope near midrapidity, becomes irrelevant.

The directed flow of particles other than nucleons has been observed. At AGS by the E895 [56] and E877 [57] collaborations there has been observed the positive directed flow of Λ hyperons in semicentral Au-Au collisions at 6.0 and 11.5 GeV/c momentum. The proton flow at forward rapidities $2.8 < Y < 3.4$, obtained by the E895 collaboration, is larger than the flow of Λ's close to midrapidity ($|Y/Y_{\rm proj}| \leq 0.6$). The average flow amplitude for Λ hyperons, obtained by the E877 collaboration, is comparable with that for protons for the same acceptance region. This result is consistent with the measurements performed at lower energies (< 2 GeV/nucleon) by EOS collaboration [58], and suggests that Λ flow follows the flow of nucleons.

In the E877 collaboration directed flow of antiprotons [59] is studied also in Au-Au collisions at a beam momentum of 11.5 GeV/nucleon. It is shown that the antiproton's directed flow is anticorrelated to proton flow.

The directed flow of fragments (d, t, ^{3}He...) has been studied at BEVALAC and SIS energies [53, 60]. Their directed flow increases with their masses. A similar behaviour at AGS energies was reported.

The systematic study of the dependence of the flow on the target/projectile mass and the beam energy represents a comprehensive body of data that should enable theoretical model calculations to obtain further information on the nuclear matter EOS. To compare the large number of different experimental results with various energies and masses seems to be a difficult task. However, the general features of the collective flow could, in principle, be expressed in terms of scale invariant quantities, as was pointed out by Balazs et al. in Ref. 61. In this way the particular differences arising from the different initial conditions, masses, energies, etc., can be separated from the general features. A way of comparing the energy dependence of flow values for different projectile/target mass combinations was suggested by A. Lang et al. [62] and first used by J. Chance in Ref. 25. To allow for different projectile/target (A_P, A_T) mass systems, they divided the flow values by $(A_P^{1/3} + A_T^{1/3})$ and called $F_s = F/(A_P^{1/3} + A_T^{1/3})$ the scaled flow. Figure 10 shows a plot of F_s versus the projectile energy per nucleon. Figure 10 represents our results and the data from EOS [25, 63], E895 [29], E877 [28], FOPI [21], NA49 [37], Propane Buble Chamber [33] experiments, along with the values derived from the Plastic Ball [55] and the Streamer Chamber [50, 51] experiments for a variety of energies and mass combinations. For the EOS and Plastic Ball data all the isotopes of $Z = 1$ and 2 are included, except for [55], where the data are given only for $Z = 1$. The Streamer Chamber data [50, 51] normally include all protons, either free or bound in clusters as in our case. The scaled flow F_s, whose value obtained below 1 GeV/nucleon of incident energy is approximately $F_s \approx 0.03 P_{\mathrm{proj}}$, reaches a maximum of 50 MeV and then decreases slowly. A first indication of this decrease between 1.0 and 2.0 GeV/nucleon was repoted in Ref. 21. It is confirmed between 2.0 and 6.0 GeV/nucleon by our results and results of Ref. 29. At 10.8 GeV/nucleon, the E877 collaboration measured $F_s = 35$ MeV [28], compatible with the value $F_s = 31 \pm 7 \pm 6$ MeV, found by E917 collaboration [30]. The fact, that F is proportional to $A_P^{1/3} + A_T^{1/3}$, i. e., to the collision time, which was predicted by macroscopic calculations [62], is an indication that the system is on its way towards thermalization, but only partially thermalized [64].

It is worth noting that the data obtained by streamer chamber technique (including our results) are slightly higher than those obtained by electronic experiments. This may be caused by a small mixture of bound protons (deuterons, ^{3}H, ^{3}He).

Several theoretical models of nucleus–nucleus collisions at high energy have been proposed. The quark gluon string model (QGSM) is used for a comparison with our experimental data. The QGSM is based on the Regge and string phenomenology of particle production in inelastic binary hadron collisions [11]. The QGSM simplifies the nuclear effects (neglects the potential interactions between hadrons, coalescence of nucleons, etc.). A detailed description and comparison of the QGSM with experimental data over a wide energy range can be found in

Refs. 11. We have generated C-Ne and C-Cu interactions using the Monte Carlo generator COLLI, based on the QGSM and then traced through the detector and trigger filter.

In the generator COLLI there are two possibilities to generate events: 1) at not fixed impact parameter $\tilde{b}$ and 2) at fixed b. From the impact parameter distributions the mean values of b have been obtained: $\langle b \rangle = 2.20$ fm for C-Ne and $\langle b \rangle = 2.75$ fm for C-Cu collisions. For the obtained values of $\langle b \rangle$ total samples of 8400 C-Ne and 9327 C-Cu events have been generated. The QGSM overestimates the production of low momentum protons with $P < 0.2$ GeV/c, which are mainly the target fragments and were excluded from the analysis. From the analysis of generated events the protons with deep angles greater than 60° have been excluded, because such vertical tracks are registered with less efficiency from the experiment. The proton multiplicity, rapidity, $\langle P_T \rangle$, and momentum distributions of generated events for fixed and not fixed $\tilde{b}$ are consistent and reproduce the data. The corresponding values of $\langle Y \rangle$ and $\langle N_p \rangle$ are listed in Table 1. The experimental and QGSM results coincide within the errors. For generated events the component in the true reaction plane P_x had been calculated. In the model calculations the reaction plane is known a priori and is referred as the true reaction plane. The dependences of $\langle P_x(Y) \rangle$ on Y are shown on Fig. 8, *a, b*. For the visual presentation, we approximated these dependences by polynoms (the curves on Fig. 8, *a, b*). From the comparison of the dependences of $\langle P_x(Y) \rangle$ on Y obtained by the model in two regimes — for fixed and not fixed $\tilde{b}$ — one can conclude that the results are consistent and it seems, that in our experiments the values of $b = 2.20$ fm for C-Ne, $b = 2.75$ fm for C-Cu are probable. The QGSM yields a significant flow signature, which follows trends similar to the experimental data. To be convinced, that the significant sidewards deflection in Fig. 8, *a, b* (for both experiment and QGSM) is due to correlations within the events, and cannot be the result of detector biases or finite-multiplicity effects, the $\langle P_x(Y) \rangle$ on Y has been obtained for events composed by randomly selecting tracks from different QGSM events (within the same multiplicity range) (Fig. 8, *a, b*). One can see from Fig. 8, *a, b*, that in these events there is no correlation with reaction plane. The dependences of $\langle P_x(Y) \rangle$ on normalized rapidity $Y/Y_{\rm proj}$ of QGSM data for fixed parameters in C-Ne ($b = 2.20$ fm) and C-Cu ($b = 2.75$ fm) collisions are presented in Fig. 9, *a, b*. The values of F, obtained from the QGSM, are listed in Table 1. One can see, that the QGSM slightly underestimates the flow at our energies. This model underestimates also the transverse flow at BEVALAC energies (1.8 GeV/nucleon) [11]. As shown by Stocker and Greiner [9], the reason, that the QGSM fails to reproduce the flow data in the energy region of $1 \div 5$ GeV/nucleon, is the neglect of mean-field effects. (In the QGSM the sidewards flow is a sole result of the rescattering of secondaries.) At higher energies the influence of a mean field is expected to be weaker, so it is believed that the QGSM will still underestimate the flow, but will give a better estimate

than at lower energies. In the framework of QGSM the transverse flow F of protons of the order of ~ 100 MeV/c has been predicted for Au-Au collisions at a momentum of 11.6 GeV/c at AGS energies. The QGSM slightly underestimated the experimental results (~ 130 MeV/c) which have been obtained later. The QGSM with proper treatment of rescattering predicted observable collective flow of protons in Pb-Pb collisions at SPS CERN energy of 160 GeV/nucleon, of the order of ~ 50 MeV/c.

We have obtained also the mean transverse momentum per nucleon in the reaction plane in the forward hemisphere of the c. m. system $\langle P_x \rangle_{y>0}$. The estimated and corrected (multiplied by $k_{\rm corr}$ factor) values of $\langle P_x \rangle_{y>0}$ are listed in Table 1. The dependence of $\langle P_x \rangle_{y>0}$ on beam energy and target/projectile mass is presented in Fig. 11. Results on central Ar-KCl [39, 64], Ar-BaI_2 [51], Ca-Ca [54, 55], Nb-Nb [55], Ar-Pb [51] collisions from the Plastic Ball, Diogene and BEVALAC streamer chamber groups are given together with our results for comparison. The $\langle P_x \rangle_{y>0}$ rises monotonously with $E_{\rm beam}$, irrespective of the projectile/target configurations. For symmetric systems (Ar-KCl, Ca-Ca, Nb-Nb) a linear rise with beam energy from $\langle P_x = \rangle_{y>0} = 50$ MeV/c at 0.4 GeV/nucleon to 95 MeV/c at 1.8 GeV/nucleon is observed. The $\langle P_x \rangle_{y>0}$ in the asymmetric system Ar-Pb, levels off above 0.8 GeV/nucleon, with data on an intermediate mass target (BaI_2) exhibiting a somewhat higher $\langle P_x \rangle_{y>0}$ at 1.2 GeV/nucleon. In Fig. 11 the Boltzmann–Uechleng–Ulenberg (BUU) transport model [65] calculations for Ar-Pb are presented. The transport models have been successful in studying various aspects of relativistic heavy-ion collisions, such as single-particle spectra, collective effects (stopping, bounce-off, squeeze-out) and meson production. The hadronic transport model was developed by solving numerically a coupled set of transport equations for the phase-space distribution functions $f(x, p)$ of nucleons, baryon resonances ($\Delta(1232)$ and $N^*(1440)$) and pions:

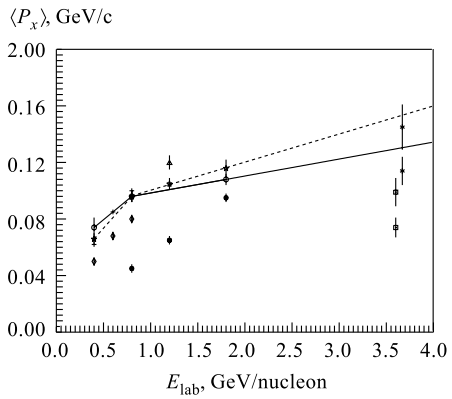

Fig. 11. The average transverse momentum per nucleon in the reaction plane in the forward hemisphere of the c.m. system as a function of beam energy for various projectile/target configurations: ○ — Ar-Pb [50]; △ — Ar-BaI_2 [51]; ◇ — Ca-Ca [54, 55]; • — Ar-KCl [39, 64]; † — Nb-Nb [55]; ⋆ — the BUU calculations for Ar-Pb [65]; □ — C-Ne; ∗ — C-Cu the estimated and multiplied on correction factor $k_{\rm corr}$. The solid and dashed lines connect experimental and BUU values of Ar-Pb and are extrapolated up to $E = 4$ GeV/nucleon

$$\frac{\partial f_b(x,p)}{\partial t} + \frac{\mathbf{p}}{E_b}\nabla_r f_b(x,p) - \nabla_r U(x)\nabla_P f_b(x,p) = I^b_{bb}(x,p) + I^b_{b\pi}(x,p), \quad (23)$$

$$\frac{\partial f_\pi(x,k)}{\partial t} + \frac{\mathbf{k}}{E_\pi}\nabla_r f_\pi(x,k) = I^\pi_{b\pi}(x,k), \quad (24)$$

where $x = (\mathbf{r}, t)$ notation is used. $p = (E, \mathbf{p})$ is the four-momentum of baryons; and $k = (E_\pi, \mathbf{k})$, of pions. The collision terms $I^b_{bb}(x,p)$ and $I^b_{b\pi}(x,p)$ are the rate of change of the baryon–baryon phase-space distribution due to baryon–baryon and baryon–pion collisions, while $I^\pi_{b\pi}(x,k)$ is the rate of change of the pion phase-space distribution function due to baryon–pion collisions. The solution to the coupled transport equations was obtained by using the test particle method [66]. The nucleons are bound in the self-consistent mean field potential U and they propagate along curved trajectories as determined by the mean field. For the potential U the momentum-dependent Yukava interactions NMDYI have been chosen [65]

$$U_(\rho, \mathbf{p}) = A\Big(\frac{\rho}{\rho_0}\Big) + B\Big(\frac{\rho}{\rho_0}\Big)^\sigma + 2\frac{C}{\rho_0}\int d^3p' \frac{f(\mathbf{r}, \mathbf{p}')}{1 + \Big(\dfrac{\mathbf{p} - \mathbf{p}'}{\Lambda}\Big)^2}, \quad (25)$$

here $f(\mathbf{r}, \mathbf{p}')$ is the phase-space density; the configuration space density $\rho = \int f(\mathbf{r}, \mathbf{p}) d^3p$. There are five constants in Eq. (25); these are found by requiring that $E/A = -16$ MeV, the normal nuclear density $\rho_0 = 0.16$ fm^{-3}, the compressibility coefficient $K = 215$ MeV, $U(\rho_0, p = 0) = -75$ MeV, and $U(\rho_0, p^2/(2m) = 300 \text{ MeV}) = 0$. Their values are then $A = 110.44$ MeV, $B = 140.9$ MeV, $C = -64.95$ MeV, $\sigma = 1.24$, $\Lambda = 1.58 p_F^0$ (the parameter Λ describes the width of the momentum distribution) and yield an effective mass $m^* = 0.67$ m at the Fermi surface.

However, for NMDYI, the full single-particle energy has the form [65]:

$$\epsilon(p) = p^2/2m + A(\rho/\rho_0) + B(\rho/\rho_0)^\sigma + R(\rho, p), \quad (26)$$

where at finite temperature $T = 1/\beta$ (β is the velocity)

$$R(\rho, p) = 2\frac{C}{\rho}\frac{4}{h^3}\int d^3p' \frac{1}{\mathrm{e}^{\beta[\epsilon(p') - \mu]} + 1} \frac{1}{1 + \Big(\dfrac{\mathbf{p} - \mathbf{p}'}{\Lambda}\Big)^2}, \quad (27)$$

where the occupation probability $n[\epsilon(p)]$ is equal to [65]:

$$n[\epsilon(p)] = \frac{1}{\mathrm{e}^{\beta[\epsilon(p) - \mu]} + 1} \quad (28)$$

for a given temperature $T = 1/\beta$ and density ρ; μ is the chemical potential.

Equation of state curves are traditionally plots of pressure P versus density ρ for constant temperature T. With known values of $n[\epsilon(p)]$ the pressure can be computed. In Ref. 65 a general expression for the pressure tensor is given. According to this expression, the equilibrium pressure P has been calculated in Ref. 65 (for NMDYI):

$$P = \frac{16\pi}{h^4}\int dp\Big(\frac{p^4}{3m} + \frac{p^3}{3}\frac{\partial U}{\partial p}\Big)n(\epsilon(p)) + \frac{A}{2}\frac{\rho^2}{\rho_0} + B\frac{\sigma}{\sigma+1}\frac{\rho^{\sigma+1}}{\rho_0^{\sigma}} +$$

$$+\frac{16\pi}{h^3}\int dpp^2R(\rho,p)n[\epsilon(p)] - \Big(\frac{4}{h^3}\Big)^2\frac{C}{\rho}\int d^3pd^3p'\frac{n(p)n(p')}{1+\Big(\frac{\mathbf{p}-\mathbf{p}'}{\Lambda}\Big)^2}, \qquad (29)$$

where U is given by Eq. (25). The compressibility coefficient K is defined in Ref. 44 as $K = 9\Big(\frac{\partial P}{\partial n}\Big)$.

The momentum dependence in (25) arises from the exchange term of a Yukava force. The Coulomb potential for protons is also included in the BUU model. For nucleon–nucleon scatterings, both elastic and inelastic channels are included by using the experimentally measured cross sections with explicit isospin dependence.

In the BUU model the dynamical mean field and momentum depedent forces are responsible for the production of sufficient repulsion in the nuclear collisions. The BUU calculations with the NMDYI reproduce well the Ar-Pb experimental result (Fig. 11) [67]. Unfortunately the BUU calculation in the energy region of 3–5 GeV/nucleon and light systems of C-Ne and C-Cu have not been carried out. Therefore the BUU results have been extrapolated (dashed line in Fig. 11) for Ar-Pb up to our energy of $\sim$ 4 GeV/nucleon. One can see, that BUU model's extrapolation reproduces our C-Cu result, but it is desirable to perform precise calculations with transport models for our experimental conditions.

3.2. Pions. Pions are copiously produced in relativistic heavy-ion collisions. Interesting information about the hot and dense hadronic matter formed transiently during the reaction can be obtained by studying the pions.

In view of the strong coupling between the nucleon and pion, it is interesting to know if pions also have a collective flow behaviour and how the pion flow is related to the nucleon flow.

The emission pattern of pions in the reaction was also studied first at BEVALAC by Streamer Chamber group [64, 68] and later at SATURNE by DIOGENE group in 0.8 GeV/nucleon Ne-nucleus collisions [69] by analyzing the average transverse momentum of pions in the reaction plane as a function of rapidity.

We have studied the flow effects of π^- mesons [52]. For this purpose the reaction plane was defined for the participant protons, and the transverse momentum of each π^- meson was projected onto this reaction plane. Figure 9, *a, b* shows the dependence of $\langle P_x \rangle$ on the normalized rapidity $Y/Y_{\rm proj}$ in the laboratory system for π^- mesons in C-Ne and C-Cu collisions. The data exhibit the typical S-shape behaviour as for the protons. The values of flow F for π^- mesons are: for C-Ne collisions $F = 29 \pm 5$ MeV; for C-Cu — $F = -47 \pm 6$ MeV. The straight lines in Figure 9 show the results of this fit. The fit was done in the following intervals of $Y/Y_{\rm proj}$: $0.04 \div 0.70$ for C-Ne; $-0.06 \div 0.60$ for C-Cu. The absolute value of F increases with the mass number of target A_T, indicating the rise of the collective flow effect. The similar tendency was observed in [69] for π^- and π^+ mesons in Ne-NaF, Ne-Nb and Ne-Pb interactions at 0.8 GeV/nucleon.

For Mg-Mg collisions (~ 6000 events) we have inclusive data — only π^- mesons (~ 50000 pions) are measured. The trigger was selecting «central» collision events defined as those without charged projectile spectator fragments and spectator neutrons ($P/Z > 3$ GeV/c) emitted at angles $\theta_{\rm ch} = \theta_n = 2.4^\circ$ (~ 4 msr) which corresponds to a stripping nucleon transverse momentum of ~ 180 MeV/c. The fraction of such events is $\approx 4 \cdot 10^{-4}$ among all inelastic interactions. Approximately $10\,\%$ of π^- mesons are lost mainly due to absorption in the target and bad measurability of vertical tracks which are located around target rapidity value of -1.1 in the Mg-Mg rest frame. As the π^- mesons are emitting mainly from decays of Δ isobars (at least $\sim 80\,\%$) [70], we decided to investigate whether a single π^- meson of the event knows something about its origin and the question whether they are collectively correlated. For this purpose the technique of P. Danielewicz and G. Odyniec has been applied to Mg-Mg data. As we have inclusive data, the $\mathbf{Q}$ vector from the $\mathbf{P}_{\perp i}$ of only π^- mesons has been constructed event by event for the events with multiplicity $n_- > 7$.

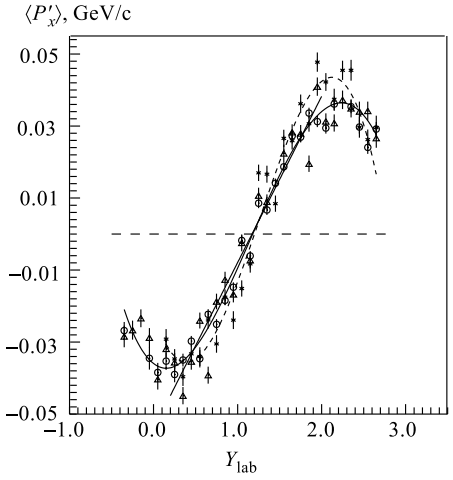

Fig. 12. The dependence of $\langle P'_x(Y) \rangle$ on $Y_{\rm lab}$ for π^- mesons in Mg-Mg collisions: $\circ$ — the experimental data; $\triangle$ — the QGSM generated data for fixed $b = 1.34$ fm; $*$ — the QGSM generated data for $\tilde{b}$. The solid line is the result of the linear approximation of experimental data in the interval of Y — $0.2 \div 2.0$. The curves for visual presentation of the QGSM events (solid — for fixed b; dashed — for not fixed $\tilde{b}$) — result of approximation by the 4th order polynomial function

According to [39], the correction factor $k_{\rm corr}$ has been defined, averaged over all the multiplicities. The value of $k_{\rm corr} = 1.51 \pm 0.05$ has been obtained.

Figure 12 shows the dependence of the estimated $\langle P'_x(Y)\rangle$ on Y for pions in Mg-Mg collisions. The data exhibit S-shape behaviour similar to the form of the $\langle P_x\rangle$ spectra for protons and pions in C-Ne and C-Cu interactions. The slope at midrapidity has been extracted from a linear fit to the data for Y between $0.2 \div 2$. The straight line in Fig. 12 shows the result of this fit. The value of F is — $F = 48 \pm 5$ MeV/c.

The QGSM have been used for the comparison with the Mg-Mg data. For not fixed impact parameter $\tilde{b}$ there have been generated 6225 events. From the b distribution the mean value of $\langle b\rangle = 1.34$ fm has been obtained and total sample of 6212 events for this $\langle b\rangle$ has been generated. For simulated events the component in the true reaction plane P_x had been calculated. The dependences of $\langle P_x(Y)\rangle$ on Y (for both $\tilde{b}$ and b) are shown in Fig. 12. One can see from Fig. 12, that the QGSM yields flow signature with similar tendency to the experimental data. For the visual presentation, we approximated these dependences by polynoms (the curves in Fig. 12). From the comparison of the dependences of $\langle P_x(Y)\rangle$ on Y obtained by the model in two regimes — for $\tilde{b}$ and b, one can conclude, that the results are consistent. The values of F, obtained from the QGSM are: $F = 53 \pm 3$ MeV/c — for not fixed $\tilde{b}$; $F = 51 \pm 4$ MeV/c — for $b = 1.34$. One can see, that the QGSM underestimates this parameter.

One can see from Fig. 9 that the proton flow is larger than the pion flow. A similar tendency has been observed at BEVALAC, GSI-SIS, AGS and CERN-SPS. The flow of nucleons has been interpreted as a recoil effect from the compression generated during the early stage of a heavy-ion collision, and its magnitude has been used to infer the compressibility of nuclear matter at high temperatures and pressures. The nucleons mostly experience elastic NN collisions, while pions generally have inelastic interactions. The pions, which are created in the dense, hot, high pressure region, are differentially scattered and reabsorbed by the intervening hadronic matter in the interaction region and in the spectators. Pions are not affected by the nuclear incompressibility as nucleons are. They are either created isotropically in individual NN collisions, or emitted in the rest frame of a decaying Δ resonance. Once created, they can either escape, scatter ($\pi^- N \to \Delta \to \pi^- N$), or be reabsorbed ($\pi^- NN \to \Delta N \to NN$).

One can see from Fig. 9, that for C-Ne collisions $\mathbf{P}_x$ for pions is directed in the same direction as for protons, i. e., flows of protons and pions are correlated, while for C-Cu ineractions the $\mathbf{P}_x$ of π^- mesons is directed oppositely to that of the protons (antiflow).

The correlation of nucleon and pion flows had been observed experimentally by the DIOGENE group for central Ne-NaF, Ne-Nb and Ne-Pb collisions ($b \leq$ 3 fm) at energy of $E = 0.8$ GeV/nucleon [68]. At BEVALAC by Streamer Chamber group the flow behaviour for pions has been obtained also in Ar-KCl, Ar-

Pb and La-La interactions [64]. These results are in agreement with our findings for C-Ne. The Propane Buble Chamber collaboration has not observed the flow of pions in C-C collisions at a momentum of 4.2 GeV/c/nucleon. Perhaps, it is too weak to be detected experimentally. At BEVALAC energy of 1.15 GeV/nucleon the antiflow of π^- and π^+ has been observed by the EOS collaboration [71] in Au-Au collisions, similarly to the observations at AGS energy of 11 GeV/nucleon by the E877 collaboration [28] in Au-Au collisions and at CERN-SPS energy of 158 GeV/nucleon by the WA98 collaboration [36] in semicentral Pb-Pb collisions. The magnitude of the directed flow in [36] is found to be significantly smaller than that observed at AGS energies. Thus, it seems, that the flow effects for pions decrease with increase of the energy.

Theoretical calculations in the framework of the isospin quantum molecular dynamics (IQMD) model [70] and the relativistic hadronic BUU transport model [72] have predicted that in Au-Au collisions with increase of the impact parameter b, the $\langle P_x \rangle$ of pions changes its sign. Therefore as reaction goes from central to semicentral and peripheral ($b \geq 3$ fm), the $\langle P_x \rangle$ distribution of pions undergoes a transition from being correlated to anticorrelated with that of nucleons.

The IQMD is a dynamical model which calculates the time evolution of a heavy-ion collision in the entire many-body phase. Nucleons are represented as Gaussian wavefunctions and their centroids are propagated according to the canonical equations of motion. If two particles approach too close in configuration space, so that $d_{jk} \leq \sqrt{\sigma/\pi}$ a hard collision is carried out in a similar fashion as in intranuclear cascades. The final state of each binary collision is checked to obey the Pauli principle. Model allows for rescattering and the formation and decay of resonances and strings. It includes explicitly 50 different baryon species (nucleon, Δ, hyperon, and their resonances) and 25 different meson species (including strange meson resonances), which are supplemented by all isospin-projected states.

Within the framework of the relativistic transport model (ART 1.0) [73] for heavy-ion collisions at AGS energies, pions are found to have a weak flow behaviour in central collisions. This enhancement in the direction of the baryonic matter for the most central events was attributed to the rescattered pions retaining some momentum from the Δ's from which they decayed. The Δ's exhibited the same flow signature as the final state nucleons [70].

The origin of the particular shape of the $\mathbf{P}_x$ spectra for pions was studied in [70, 72, 73]. The investigation revealed that the origin of the in-plane transverse momentum of pions is the pion scattering process (multiple πN scattering) [70] and the pion absorption [72]. The $\langle P_x \rangle$ distribution of pions is not a collective effect in the sense of the nucleonic bounce-off: the observable is the same, but the cause is different. The final pion P_x distribution therefore reflects the complicated reaction dynamics of pion production, reabsorption, rescattering as well as the collective flow of baryon resonances.

The anticorrelation of nucleons and pions was explained in [70] as due to multiple πN scattering. However, in [72, 73] it was shown, that anticorrelation is a manifestation of the nuclear shadowing effect of the target and projectile spectators through both pion rescattering and reabsorptions. In our opinion, our results indicate that the flow behaviour of π^- mesons in a light system C-Ne is due to the flow of Δ resonances, whereas the antiflow behaviour in a heavier C-Cu system is the result of the nuclear shadowing effect.

The flow behaviour of other mesons, namely K^+ and K^0, has been observed also. Experimental data on K^+-meson sideward flow, measured with the FOPI detector at SIS/GSI in the reactions Ru-Ru at 1.69 GeV/nucleon, and Ni-Ni at 1.93 GeV/nucleon have been obtained [74]. The K^+-sideward flow is found to be anticorrelated with the one of protons. For heavy-ion collisions at higher energies available from the AGS, the directed flow of K^0 mesons in Au-Au collisions at a momentum of 6 GeV/nucleon was studied experimentally by the E895 collaboration [75]. Preliminary data have shown that neutral kaons have a strong antiflow relative to that of nucleons.

4. AZIMUTHAL ANISOTROPIC EMISSION OF PROTONS AND PIONS

The preferential emission of particles in the direction perpendicular to the reaction plane (i. e., «squeeze-out») is particularly interesting since it is the only way the nuclear matter might escape without being rescattered by spectator remnants of the projectile and the target, and is expected to provide direct information on the hot and dense participant region formed in high energy nucleus–nucleus ineractions. This phenomenon was predicted by hydrodynamical calculations [4], and first has been confirmed for charged particles by the Plastic-Ball collaboration [16, 76]. Then this effect was clearly identified in the experiments at GSI set-ups KAOS [77], TAPS [78], FOPI [79], KAON [24], LAND [22] and DIOGENE group at SATURNE by the observation of an enhanced out-of-plane emission of protons, neutrons, mesons, and charged fragments.

In order to extend these investigations, the azimuthal angular distributions (ϕ) of the protons and pions in C-Ne and C-Cu collisions have been studied. The angle ϕ is the angle of the transverse momentum of each particle in an event with respect to the reaction plane ($\cos\phi = P_x/P_t$). The reaction plane is the plane containing the vector $\mathbf{Q}$ and the beam axis (see Sect. 2.1). The analysis was restricted only to the midrapidity region by applying a cut around the centre-of-mass rapidity. Figure 13, *a, b* shows distributions for protons and π^- mesons in C-Ne and C-Cu collisions. For visual presentation the data on C-Cu were shifted upwards. For π^- mesons the analysis was performed from 0 to 180° due to lower statistics than for protons. The azimuthal angular distributions for the protons and pions show maxima at $\phi = 90°$ and 270° with respect to the

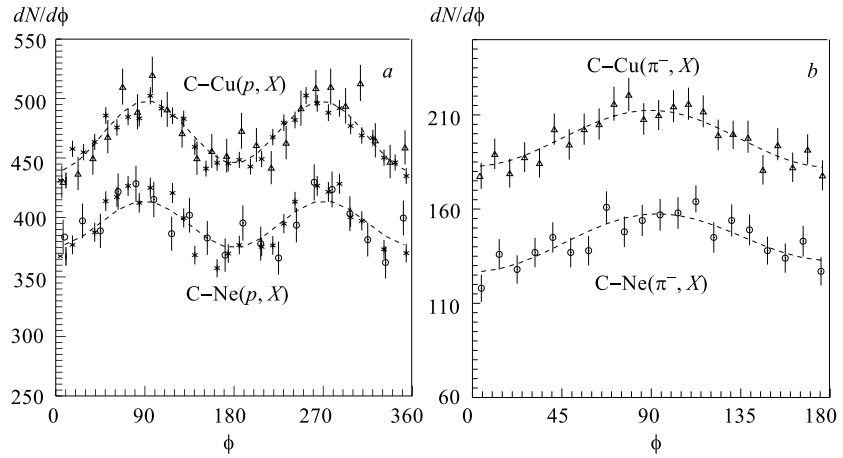

Fig. 13. The azimuthal distributions with respect to the reaction plane of midrapidity protons $dN/d\phi$ (*a*) and π^- mesons (*b*): $\circ$ — for C-Ne ($-1 \leq y_{\rm c.m.} \leq 1$); $\triangle$ — for C-Cu ($-1 \leq y_{\rm c.m.} \leq 1$) interactions; $*$ — the QGSM data. Also shown are the fits using the function $dN/d\phi = a_0(1 + a_1 \cos\phi + a_2 \cos 2\phi)$

event plane. These maxima are associated with preferential particle emission perpendicular to the reaction plane (squeeze-out, or elliptic flow). Thus a clear signature of an out-of-plane signal is evidenced.

To treat the data in a quantitative way the azimuthal distributions were fitted by a polynomial:

$$\frac{dN}{d\phi} = a_0(1 + a_1 \cos\phi + a_2 \cos 2\phi). \tag{30}$$

The anisotropy factor a_2 is negative for out-of-plane enhancement (squeeze-out) and is the measure of the strength of the anisotropic emission. The values a_2 are affected by the uncertainty in determining the reaction plane due to the finite multiplicity. The true values of a_2 can, however, be derived by multiplying the fitted values of a_2 by the correction factor [45]:

$$a_2^{\rm corr} = a_2/\langle\cos 2\Delta\phi\rangle. \tag{31}$$

The correction factor $\langle\cos 2\Delta\phi\rangle$ has been estimated using the method proposed by Ollitrault [45] (see Sect. 2.2). $\langle\cos 2\Delta\phi\rangle$ is determined from the $\langle\cos\phi_{12}\rangle$ following the prescription outlined in Ref. 45. The values of $\langle\cos 2\Delta\phi\rangle$ are: $\langle\cos 2\Delta\phi\rangle = 0.825$ for C-Ne interactions and $\langle\cos 2\Delta\phi\rangle = 0.795$ for C-Cu. The corrected a_2 coefficients are presented in Table 2. The fitted curves are superimposed on the experimental distributions (Fig. 13).

Table 2. **The values of the parameter a_2 and the ratio R for protons and π^- mesons**

$A_p - A_T$	Particle	Applied Cut	a_2	R
C-Ne	Protons (QGSM)	$-1 \leq y_{\mathrm{c.m.}} \leq 1$	-0.025 ± 0.005	1.05 ± 0.04
	Protons (exp.)	$-1 \leq y_{\mathrm{c.m.}} \leq 1$	-0.049 ± 0.014	1.10 ± 0.03
		$-1 \leq y_{\mathrm{c.m.}} \leq 1$; $P_T \geq 0.3$ GeV/c	-0.074 ± 0.014	1.16 ± 0.04
	π^- mesons	$-1 \leq y_{\mathrm{c.m.}} \leq 1$	-0.035 ± 0.013	1.07 ± 0.04
		$-1 \leq y_{\mathrm{c.m.}} \leq 1$; $P_T \geq 0.1$ GeV/c	-0.050 ± 0.014	1.09 ± 0.03
C-Cu	Protons (QGSM)	$-1 \leq y_{\mathrm{c.m.}} \leq 1$	-0.058 ± 0.004	1.12 ± 0.01
	Protons (exp.)	$-1 \leq y_{\mathrm{c.m.}} \leq 1$	-0.065 ± 0.014	1.14 ± 0.04
		$-1 \leq y_{\mathrm{c.m.}} \leq 1$; $P_T \geq 0.3$ GeV/c	-0.081 ± 0.014	1.18 ± 0.05
		$-0.6 \leq y_{\mathrm{c.m.}} \leq 0.6$	-0.077 ± 0.017	1.17 ± 0.04
		$-0.6 \leq y_{\mathrm{c.m.}} \leq 0.6$; $P_T \geq 0.3$ GeV/c	-0.088 ± 0.020	1.19 ± 0.06
	π^- mesons	$-1 \leq y_{\mathrm{c.m.}} \leq 1$	-0.041 ± 0.013	1.08 ± 0.03
		$-1 \leq y_{\mathrm{c.m.}} \leq 1$; $P_T \geq 0.1$ GeV/c	-0.056 ± 0.015	1.12 ± 0.04

The quark-gluon string model (QGSM) has been used for the comparison with the experimental results. The QGSM data for protons at fixed impact parameter in C-Ne ($b = 2.20$ fm) and C-Cu ($b = 2.75$ fm) are also superimposed in Fig. 13 and corresponding values of a_2 extracted from the QGSM data are listed in Table 2. One can see, that the model describes the experimental azimuthal distributions.

The values of a_2 are used to quantify the ratio R of the number of particles emitted in the perpendicular direction to the number of particles emitted in the reaction plane, which represents the magnitude of the out-of plane emission signal:

$$R = \frac{1 - a_2}{1 + a_2}. \tag{32}$$

A ratio R larger than unity implies a preferred out-of-plane emission. The values of R are listed in Table 2. One can see, that a_2 and R are increasing for both protons and π^- mesons, with increasing the transverse momentum and the mass number of target A_T and also with narrowing of the cut applied around the centre-of-mass rapidity. The squeeze-out effect is more pronounced for protons

than for π^- mesons. Our results on rapidity, mass and transverse momentum dependence of the azimuthal anisotropy are consistent with analysis from Plastic Ball [16, 76], FOPI [79] in Ni-Ni, Xe-CsI, Au-Au collisions from 0.15 to 1.0 GeV/nucleon for protons, light fragments and $\pi^{\pm}$ mesons; KAOS [77] in Au-Au at 1.0 GeV/nucleon for protons, light fragments, pions and kaons; KAON [24] in Bi-Bi collisions at 0.4, 0.7 and 1.0 GeV/nucleon for $\pi^{\pm}$ mesons; TAPS [78] collaboration in Au-Au collisions at 1.0 GeV/nucleon for π^0 mesons and are confirmed by IQMD [80] calculations. Significant squeeze-out was observed for relativistic particles (s particles — singly charged relativistic particles with velocities $\beta > 0.7$) with pseudorapidity $\eta \approx \eta_{\mathrm{c.m.}}$ in Kr-Ag(Br) collisions at energy of 0.95 GeV/nucleon of JINR emulsion experiment [32]. They have obtained for anisotropy coefficient the value of $a_2 = -0.187 \pm 0.050$.

The squeeze-out of nucleons perpendicular to the reaction plane is due to the high compression of nuclear matter in the central hot and dense reaction zone (it is genuinely collective effect, increasing linearly with A). Since the Δ resonances are expected to flow with the nucleons a similar anisotropy effects could be exhibited by their decay products, the pions. According to the microscopic transport model BUU [72], the mechanism of the azimuthal anisotropy of pions is found to be the shadowing effect of the spectator matter through both pion reabsorptions and rescatterings.

Reabsorption and rescattering of pions are stronger in plane than out of plane due to the nuclear matter located in the reaction plane. Pions emitted into the reaction plane can be absorbed and reemitted isotropically with a lower average kinetic energy. This causes a net decrease of pion abundance in the event plane for high momentum pions. Perpendicular to the reaction plane there is no spectator matter and pions with high P_t can leave the reaction zone without further interaction. The IQMD model favours the pion reabsorption as the origin [70] of anisotropy. In Ref. 77 it had been argued, that at least part of the pion squeeze could be due to the decay kinematics of the baryon resonances.

In experiments E895 [56], E877 [28] at AGS and NA49 [37] at CERN SPS the elliptic flow is typically studied at mid rapidity and is quantified in terms of the second Fourier coefficient

$$v_2 = \langle \cos\, 2\phi \rangle. \tag{33}$$

The Fourier coefficient v_2 is related to a_2 via

$$v_2 = a_2/2. \tag{34}$$

We have estimated v_2 both for C-Ne and C-Cu. The dependence of the elliptic flow excitation function (for protons) on energy E_{lab} is displayed in Fig. 14.

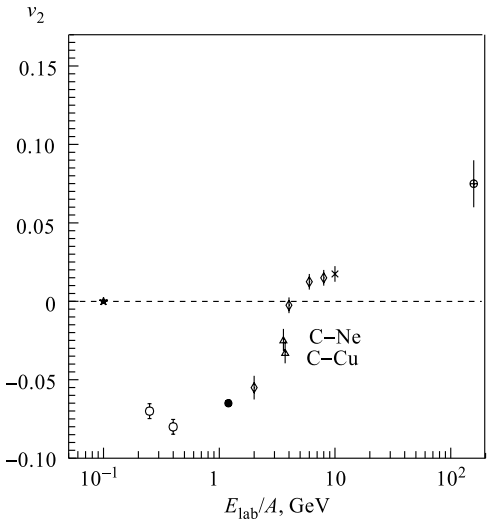

Fig. 14. The dependence of the elliptic flow excitation function v_2 on energy $E_{\rm lab}/A$ (GeV): $\star$ — FOPI; $\circ$ — MINIBALL; $\bullet$ — EOS; $\diamond$ — E895; $*$ — E877; $\oplus$ — NA49; $\triangle$ — C-Ne, C-Cu (our results)

At energies of 1–11 GeV/nucleon, the elliptic flow results from a strong competition between squeeze-out and in-plane flow [81]. In the early stages of the collision the spectator nucleons block the path of participant hadrons emitted toward the reaction plane, therefore the nuclear matter is initially squeezed out preferentially orthogonal to the reaction plane. This squeeze-out of nuclear matter leads to negative elliptic flow ($v_2 < 0$). In the later stages of the reaction, the geometry of the participant region (i. e., a larger surface is exposed in the direction of the reaction plane) favours in-plane preferential emission and hence positive elliptic flow ($v_2 > 0$). The magnitude and the sign of the elliptic flow depend on two factors [81]:

1) the pressure built up in the compression stage compared to the energy density, and

2) the passage time for removal of the shadowing due to the projectile and target spectators.

The characteristic time for the development of expansion perpendicular to the reaction plane is $\sim R/c_s$, where c_s is the speed of sound $c_s = \sqrt{\dfrac{\partial P}{\partial e}}$, R is the nuclear radius, P is the pressure, e is the energy density. The passage time is $\sim 2R/(\gamma_0 v_0)$, where v_0 is the c. m. spectator velocity. The squeeze-out

contribution of the elliptic flow should reflect the time ratio [81]

$$\frac{c_s}{\gamma_0 v_0}. \tag{35}$$

According to (35), the squeeze-out contribution should drop with the increase of energy, because of the rise in v_0 and then in γ_0. The (35) gives hope that, significant changes in the dependence of pressure on energy density, such as associated with a phase transition might be revealed in the variation of the elliptic flow. Overall, the squeeze-out contribution should decrease as a function of energy with the flow becoming positive, $v_2 > 0$. Recent calculations have made specific predictions for the beam energy dependence of elliptic flow for nucleus–nucleus (Au-Au) collisions at 1–11 GeV/nucleon [41, 81, 82]. They indicate a transition from negative to positive elliptic flow at a beam energy of $E_{\rm tr}$, which has a marked sensitivity to the stiffness of the EOS. In addition, they suggest that a phase transition to the quark-gluon plasma (QGP) should give a characteristic signature in the elliptic flow excitation function due to the significant softening of the EOS. In Fig. 14 are presented the values of v_2 obtained for protons by FOPI [79], MINIBALL, EOS [25], E895 [29], E877 [28], NA49 [37] collaborations together with our results for C-Ne and C-Cu collisions. The Propane Buble Chamber collaboration of JINR (Dubna) observed the small elliptic flow for both protons and π^- mesons in C-C collisions at a momentum of 4.2 GeV/c/nucleon [33]. It was found [33], that the elliptic flow depends on rapidity and that around the beam and target rapidities it is positive ($v_2 > 0$) for protons and negative ($v_2 < 0$) for pions. Recently the STAR collaboration obtained [38], that the elliptic flow signal, v_2, of charged particles in Au-Au collisions at RHIC at the energy of $\sqrt{s_{NN}} = 130$ GeV reaches values of about 6 % (0.06) for relatively peripheral collisions and decreases for the more central collisions. Elliptic flow appears to be independent of pseudorapidity in the region $|\eta| \leq 1.3$. Its p_t dependence is almost linear in the region $0.1 < p_t < 2$ GeV/c [38]. They found [38], that elliptic flow is underpredicted by RQMD by a factor of more than 2.

One can see from Fig. 14 that the excitation function v_2 clearly shows an evolution from negative to positive elliptic flow within the region of $2 \leq E_{\rm beam} \leq 8$ GeV/nucleon, i. e., the transition from out-of-plane enhancement to preferential in-plane emission and point to apparent transition energy $E_{\rm tr} \sim 4$ GeV/nucleon. The elliptic flow at AGS for Au-Au (E895 at 6.0, 8.0 GeV/nucleon and E877 at 10.8 GeV/nucleon) and at the SPS for Pb-Pb collisions shows in-plane enhancement, both for protons and pions in the full rapidity range. Studies based on transport models have indicated that the value for $E_{\rm tr}$ depends on the nuclear EOS at high densities [82]. Using a relativistic Boltzmann-equation transport model (BEM) of P. Danielewicz et al. [81] for comparison with experimental data of EOS-TPC, E895, E877, it has been found a softening of the EOS from a stiff form ($K \sim 380$ MeV) for beam energies below $E_{\rm tr}$ to a softer form

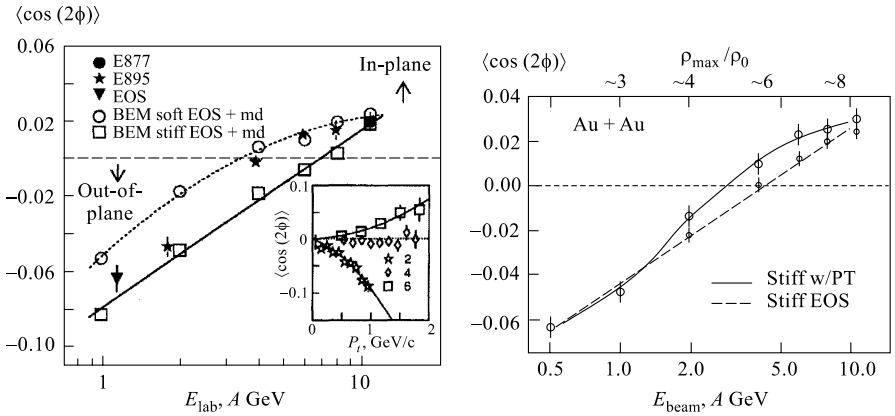

Fig. 15. Elliptic flow excitation function for Au-Au. The data are from E877, E895 and EOS collaborations. Calculations have been carried out for the soft and the stiff EOS with momentum dependence (md) (figure is from Ref. 56)

Fig. 16. Calculated elliptic flow excitation functions for Au-Au. The open diamonds represent results obtained with a stiff EOS. The open circles represent results obtained with a stiff EOS and with a second-order phase transition. The solid and dashed lines are drawn to guide the eye. Numbers at the top of the figure indicate rough magnitude of local baryon densities reached in reactions at different beam energies (figure is taken from Ref. 81)

($K \sim 210$ MeV) for beam energies above $E_{\rm tr}$ [56] (Fig. 15). Meanwhile the relativistic transport model of B. A. Li et al. [73] (ART 1.0) shows that the experimental data are consistent, instead, with the predictions using a stiff EOS without involving a softening.

In order to search for an elliptic flow signature that can be a signal of the onset of a phase transition to the QGP, in Ref. 81, there have been carried out calculations for Au-Au in the energy range of (0.5–11) GeV/nucleon assuming an EOS with a weak second-order phase transition. The elliptic flow excitation functions calculated using a stiff EOS with a phase transition (open circles) and a stiff EOS without the phase transition (diamonds) are compared in Fig. 16 (figure from Ref. 81). Both functions have been obtained with no consideration of momentum dependence in the mean field. For low beam energies (≤ 1 GeV), the elliptic flow excitation functions are essentially identical because the two EOS are either identical or not very different at the densities and temperatures that are reached. For $4 \leq E_{\rm beam} \leq 9$ GeV/nucleon the excitation function shows larger in plane elliptic flow from the calculation which includes the phase transition, indicating that a softening of the EOS has occurred for this beam energy range. This deviation is in direct contrast to the essentially logarithmic beam energy

dependence obtained from the calculations which assume a stiff EOS without the phase transition. This difference in the predicted excitation functions could very well serve as an important hint as to whether or not the conditions necessary for the phase transition to the QGP are created in this energy range.

5. THE P_T DEPENDENCE OF TRANSVERSE FLOW IN C-Ne AND C-Cu COLLISIONS

In Refs. 83, 84 there was suggested the complementary approach to the standard transverse momentum analysis of P. Danielewicz and G. Odyniec. This approach allows one to extract information about the strength of transverse flow by studying the ratio of the transverse momentum spectra $R(P_t) = (dN^+/dP_t)/(dN^-/dP_t)$, where $N^+(N^-)$ is the number of particles in the reaction plane emitted in the same (opposite) directions of sideward flow, as a function of P_t near the projectile rapidity. Although this approach is similar in spirit to that for studying the «squeeze-out» phenomenon, but has the advantage of requiring particle identification only at a single rapidity. It is interesting to investigate whether this approach can reveal new features of the transverse flow.

In Ref. 84 the variation of the strength of flow has been examined as a function of transverse momentum using both a simple, transversely moving thermal model and a more realistic, transport model [73].

In the thermal model [84] it has been assumed, that all or a fraction of particles in a small rapidity bin around Y_{proj} are in local thermal equilibration at a temperature T and the centre of mass of these particles is moving with velocity β along the direction $+x$ in the reaction plane [84]:

$$\beta = \frac{\sum\limits_i (P_x)_i}{\sum\limits_i E_i} = \frac{\sum\limits_i (P_x)_i}{\sum\limits_i (m_t)_i \cosh(Y)} \leq \frac{\langle P_x \rangle}{m_n \cosh(Y)}, \tag{36}$$

where $\langle P_x \rangle$ is the average transverse momentum per nucleon in the reaction plane, and m_n is the nucleon mass. Using the Boltzmann distribution for the thermal source and boosting it with the transverse velocity β, one obtains the following spectrum

$$\frac{d^3N}{P_t dP_t d\phi dY} = C\gamma(E - \beta P_t \cos(\phi)) \exp(-\gamma(E - \beta P_t \cos(\phi))/T), \tag{37}$$

where C is the normalization constant and ϕ is the azimuthal angle with respect to the reaction plane. The transverse momentum spectra in a small rapidity bin around Y_{proj} in the rection plane for particles emitted in the same $(dN^+/P_t dP_t)$

and opposite ($dN^-/P_t dP_t$) directions of the transverse flow are therefore given by

$$\frac{dN_\pm}{P_t dP_t} = C_\pm \mathrm{e}^{-\gamma E/T}(\gamma E \mp T\alpha)\mathrm{e}^{\pm\alpha}, \tag{38}$$

where $\alpha = \gamma\beta P_t/T$. These distributions reduce to simple exponents at high transverse momenta

$$\frac{dN_\pm}{P_t dP_t} \propto \exp\left(-P_t/T_{\mathrm{eff}}^\pm\right), \tag{39}$$

where the inverse slopes or effective temperatures $T_{\mathrm{eff}}^\pm$ in the semilogarithmic plot of the spectra at high P_t are obtained as

$$\frac{1}{T_{\mathrm{eff}}^\pm} = -\lim_{P_t\to\infty}\left[\frac{d}{dP_t}\ln\Big(\frac{dN^\pm}{P_t dP_t}\Big)\right] = \frac{\gamma}{T}\Big(\cosh(Y) \mp \beta\Big). \tag{40}$$

In general, the inverse slope $1/T_{\mathrm{eff}}^\pm$ reflects combined effects of the temperature T and transverse flow velocity β. For the special case of particles at midrapidity, β is zero and the effective temperatures are equal to the local temperature T of the thermal source. Otherwise, one expects $T_{\mathrm{eff}}^+ > T_{\mathrm{eff}}^-$. For high energy heavy-ion collisions in the region of 1–10 GeV/nucleon, β is much smaller than $\cosh(Y)$ around the projectile rapidity, and one again expects $T_{\mathrm{eff}}^+ \approx T_{\mathrm{eff}}^-$, i. e., two approximately parallel spectra $dN^+/P_t dP_t$ and $dN^-/P_t dP_t$ at high transverse momenta.

The degree of azimuthal asymmetry or the strength of transverse flow is expressed in Ref. 84 in terms of the ratio

$$R(P_t) = \frac{dN^+/P_t dP_t}{dN^-/P_t dP_t} = \frac{C_+}{C_-}\frac{1-\beta\dfrac{P_t}{E}}{1+\beta\dfrac{P_t}{E}}\ \exp\left(2P_t\frac{\gamma\beta}{T}\right). \tag{41}$$

It is seen that the ratio increases as a function of P_t for any fixed values of T and β. It is however important to stress that in reality particles are emitted continuously at different freeze-out temperatures during the whole reaction process. In particular, particles with high P_t are mostly emitted from the most violent space-time regions where the local temperatures are high. Since the ratio $R(P_t)$ varies slowly with the transverse momentum for low β/T, one thus expects in dynamical model calculations a weaker P_t dependence of the ratio $R(P_t)$ at high transverse momenta. Similar results have been obtained in the framework of the hadronic transport BUU model (ART 1.0) [73]. Namely it has been obtained [84], that the spectra at high P_t for particles moving in the same and opposite

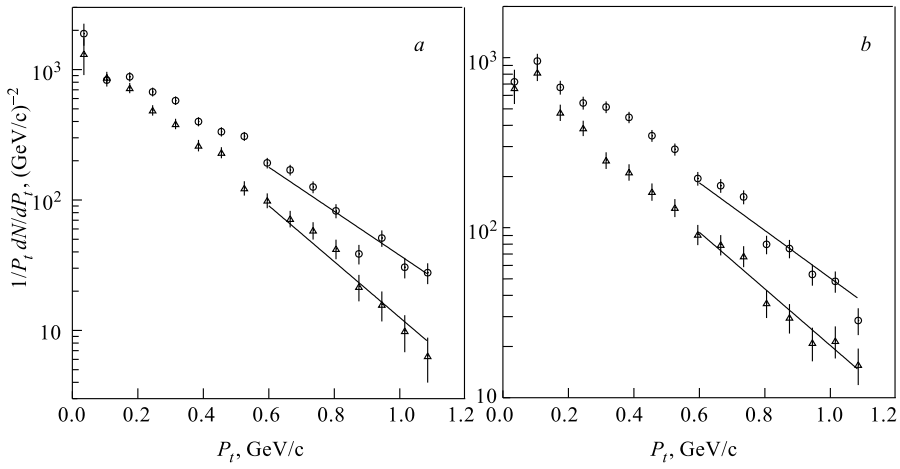

Fig. 17. The transverse momentum distributions of protons emitted in the reaction plane to the same (○) and opposite (△) side of the transverse flow in C-Ne (*a*) and C-Cu (*b*) collisions. The lines — results of the fitting by the exponents

directions of the transverse flow are approximately parralel to each other, $R(P_t)$ ratio increases gradually and reaches a limiting value at high P_t, which is very sensitive to the EOS.

We have studied the correlations between the protons detected on the same and opposite side of the sideward flow in central C-Ne and C-Cu interactions. The transverse momentum distributions for protons, emitted in the reaction plane at the rapidity intervals of $1.7 < Y < 2.4$ for C-Ne and $1.3 < Y < 2.7$ for C-Cu collisions, are shown in Fig. 17. The chosen rapidity range is around of the projectile rapidity $Y_{\rm proj} = 2.28$. In this rapidity range particles with high transverse momenta must have suffered very violent collisions and thus originate mostly from the very hot and dense participant region where large density gradients exist. On the other hand, particles with low transverse momentum are mostly from cold spectators.

From Fig. 17 one can see a very clear excess of protons emitted on the same side as the directed flow for both C-Ne and C-Cu collisions. In both collisions the spectra show typical exponential behaviour for $P_t \geq 0.6$ GeV. The spectra at high P_t for particles in the same and opposite directions of the transverse flow are approximately parallel to each other, similar to the results of the E877 collaboration for protons in Au-Au collisions at AGS energy of 10.8 GeV/nucleon and theoretical predictions of Ref. 84 on the basis of the transversely moving thermal model and hadronic transport BUU model.

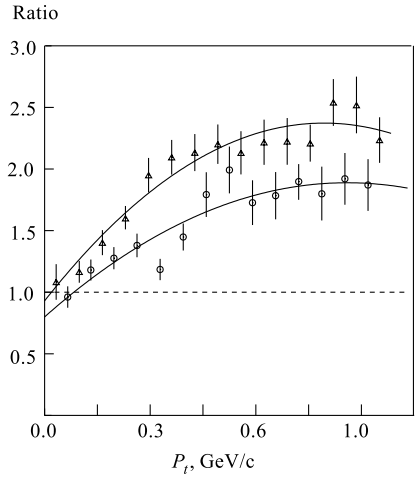

Fig. 18. Ratios of the yield of protons emitted to the same and opposite side of the transverse flow as a function of P_t in C-Ne (○) and C-Cu (△) collisions. The curves — results of the logarithmic fits to guide the eyes

In Fig. 18 the ratios $R(P_t)$ of the two spectra as a function of P_t for C-Ne and C-Cu collisions are presented in order to study the strength of the transverse flow. As expected from Ref. 84, the ratios increase gradually at low P_t and reach a limiting value of 1.9 at $P_t = 1$ GeV/c in C-Ne and 2.5 in C-Cu collisions. The limiting value in C-Cu collisions is larger than that in C-Ne collisions. For protons, the value of the ratio is greater than one $R(P_t) > 1$ at all transverse momenta. It is an unambiguos signature of the existence of sideward flow, indicating that for all P_t values the protons are emitted preferentially in the direction of the flow. The similar result has been obtained by the E877 collaboration for protons in Au-Au collisions at the energy of 10.8 GeV/nucleon. It has been found that ratio $R(P_t) > 1$ increases with P_t and reaches about 2 at $P_t = 1$ GeV/nucleon.

As the transverse momentum decreases, $R(P_t)$ is increasingly more affected by particles from cold spectators, and the ratio R approaches one as P_t goes to zero (see Fig. 18).

Since $R(P_t)$ at high P_t is very sensitive measure of the quantity β/T, and the local temperatures during the reaction process using the cascade and the soft equation of state (EOS) are almost identical [73], one expects that $R(P_t)$ depends strongly on the EOS of the superdense hadronic matter formed in the most violent stage of the reaction. This has been clearly found in Ref. 84 (see Fig. 19) by comparing results obtained using the pure cascade and the soft EOS for central collisions. On can see from Fig. 19, that although there is no significant difference between the two values of $R(P_t)$'s for $P_t \leq 0.2$ GeV/c, they differ by about a factor of 1.5 at higher P_t. Moreover, the ratios are constant within a large range of high transverse momenta.

In Fig. 20 the ratios $R(P_t)$ as a function of P_t for π^- mesons in C-Ne and C-Cu interactions at $1.0 < Y < 2.5$ are presented. In C-Ne collisions the ratio is greater than one, increases almost linearly with P_t and reaches about 1.2 at $P_t = 0.9$ GeV/c. However, an anisotropy is observed for π^- mesons in C-Cu collisions, which on average show the ratio smaller than one. This is shown by the lines in Fig. 20 which are linear fits to the data. Thus, in C-Ne interactions

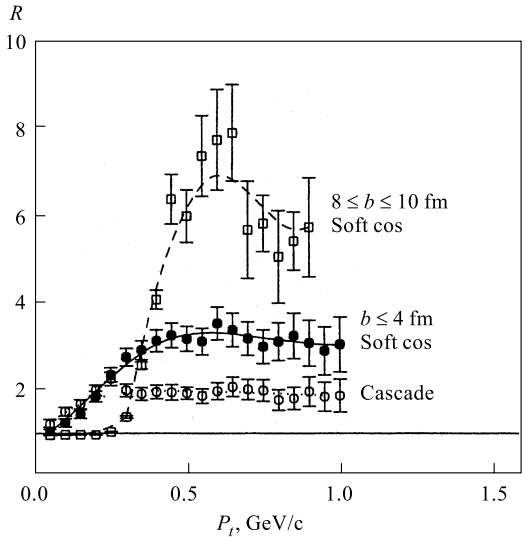

Fig. 19. Transverse momentum dependence of the strength of transverse flow in the reaction plane for particles emitted in the same/opposite side of transverse flow in reaction of Au-Au at an energy of 10.8 GeV/nucleon. Results using the soft equation of state and the pure cascade mode of ART are compared for central collisions (figure taken from Ref. 84)

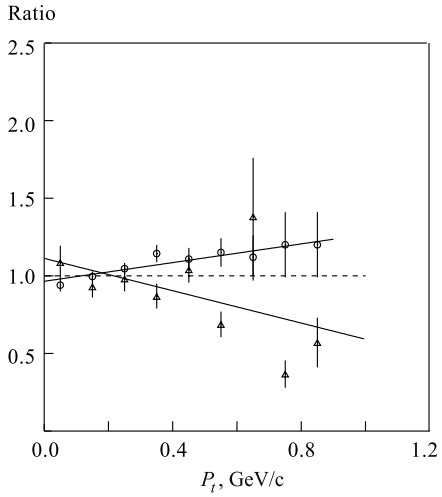

Fig. 20. Ratios of the yield of π^- mesons emitted to the same and opposite side of the transverse flow as functions of P_t in C-Ne (○) and C-Cu (△) collisions. The lines — results of fitting to guide the eyes

the pions are preferentially emitted in the direction of the flow, meanwhile in C-Cu interactions the pions are preferentially emitted away from the direction of the flow. The preferential emission of π^+ mesons away from the direction of the flow has been observed by E877 collaboration in Au-Au interactions [73] at AGS energy, selecting events with very high directivity $D > 0.12$, where $D = (E_x^2 + E_y^2)^{1/2}/E_t$. This is in qualitative agreement with the predictions of RQMD [80].

SUMMARY

Detailed experimental analysis, carried out with large acceptance detectors at BEVALAC, GSI/SIS, Dubna, Brookhaven AGS, RHIC, and CERN/SPS, allowed to obtain a clear evidence of the directed and elliptic flow effects in nuclear collisions. The measurement of flow phenomena provides direct insight into final state interactions, which can only be deduced indirectly from inclusive distributions. Therefore flow observables are important tools for investigating properties of nuclear matter under extreme conditions of high density and temperature.

The directed flow becomes smaller as the bombarding energy increases, meanwhile the in-plane (positive) elliptic flow becomes larger. Data on the proton elliptic flow from Dubna and AGS (EOS, SKM-200-GIBS, E895 and E877 collaborations) show a transition from negative (out-of-plane) to positive (in-plane) elliptic flow at a beam energy of $E_{\rm tr} \sim 4$ GeV/nucleon. Studies based on transport models have indicated that the value for $E_{\rm tr}$ depends on the nuclear EOS at high densities. Using a relativistic Boltzmann-equation transport model (BEM) it has been found a softening of the EOS from a stiff form for beam energies below $E_{\rm tr}$ to a softer form for beam energies above $E_{\rm tr}$. Such a softening of the EOS could result from a number of effects, one of which is the possible quark-gluon plasma (QGP) phase transition of nuclear matter. Meanwhile the relativistic transport model ART 1.0 shows that the experimental data are consistent instead with the prediction using a stiff EOS without involving a softening. Within this model it has been shown, that by studying the nucleon and pion elliptic flow as a function of beam energy and transverse momentum, one can obtain much more information about the reaction dynamics and the origin of the transition in the sign of elliptic flow. The results clearly show, that elliptic flow measurements can provide an important constraint on the EOS of high density nuclear matter.

For clarification of different predictions additional experimental signatures as well as calculations based on other models will be necessary.

Acknowledgements. The authors are indebted to M. Anikina, A. Golokhvastov, S. Khorozov, J. Lukstins, L. Okhrimenko, and G. Taran for fruitful collaboration during the obtaining of the data. The authors are very grateful to N. Amelin for providing them with the QGSM code program COLLI. The authors would

like to thank P. Danielewicz and Bao-An Li for the interest to their results and very valuable advices.

REFERENCES

1. *Stöcker H., Müller B.* LBL preprint 12471. Unpublished.
2. *Schied W., Ligensa R., Greiner W.* // Phys. Rev. Lett. 1968. V. 21. P. 1479;
   Schied W., Ligensa R., Greiner W. // Phys. Rev. Lett. 1974. V. 32. P. 741.
3. *Stöcker H., Maruhn J. A., Greiner W.* // Phys. Rev. Lett. 1980. V. 44. P. 725.
4. *Stöcker H. et al.* // Phys. Rev. C. 1982. V. 25. P. 1873.
5. *Buchwald G. et al.* // Phys. Rev. Lett. 1984. V. 52. P. 1594.
6. *Hartnack C. et al.* // Nucl. Phys. A. 1992. V. 538. P. 53c;
   Hartnack C. et al. // Mod. Phys. Lett. A. 1994. V. 9. P. 1151.
7. *Hofmann J. et al.* // Phys. Rev. Lett. 1976. V. 36. P. 88.
8. *Pielert G., Stöcker H., Greiner W.* // Rep. Prog. Phys. 1994. V. 57. P. 533.
9. *Schied W., Greiner W.* // Phys. Rep. 1986. V. 137. P. 277.
10. *Van Hove L.* // Phys. Lett. B. 1982. V. 118. P. 138.
11. *Amelin N. S., Staubo E. F., Csernai L.* // Phys. Rev. Lett. 1991. V. 67. P. 1523;
    Amelin N. S. et al. // Nucl. Phys. A. 1992. V. 544. P. 463c;
    Bravina L. V. et al. // Nucl. Phys. A. 1994. V. 566. P. 461c;
    Bravina L. V. et al. // Phys. Lett. B. 1995. V. 344. P. 49.
12. *Brachmann J. et al.* // Nucl. Phys. A. 1977. V. 619. P. 391.
13. *Hung C. M., Shuryak E. V.* // Phys. Rev. Lett. 1995. V. 75. P. 4003.
14. *Gustafsson H. A. et al.* // Phys. Rev. Lett. 1984. V. 52. P. 1590.
15. *Doss K. G. et al.* // Phys. Rev. C. 1986. V. 57. P. 302.
16. *Gutbrod H. H. et al.* // Phys. Lett. B. V. 216. P. 267;
    Gutbrod H. H. et al. // Phys. Rev. C. 1990. V. 42. P. 640.
17. *Renfordt R. et al.* // Phys. Rev. Lett. 1984. V. 53. P. 763.
18. *Gosset J. et al.* // Phys. Lett. B. 1990. V. 247. P. 233.
19. *Demoulins M. et al.* // Phys. Rev. Lett. 1989. V. 62. P. 1251;
    Demoulins M. et al. // Phys. Lett. B. 1990. V. 241. P. 476.
20. *Ramillien V. et al.* // Nucl. Phys. A. 1995. V. 587. P. 802.
21. *Herrmann N. et al.* // Nucl. Phys. A. 1996. V. 610. P. 49.
22. *Leifels Y. et al.* // Phys. Rev. Lett. 1993. V. 71. P. 963.
23. *Kugler A. et al.* // Phys. Lett. B. 1994. V. 335. P. 319.
24. *Brill D. et al.* // Z. Phys. A. 1997. V. 357. P. 207.
25. *Chance J. et al.* // Phys. Rev. Lett. 1997. V. 78. P. 2535;
    Partlan M. D. et al. // Phys. Rev. Lett. 1995. V. 75. P. 2100.
26. *Westfall G. D. et al.* // Phys. Rev. Lett. 1993. V. 71. P. 1986.
27. *Barrette J. et al.* // Phys. Rev. Lett. 1994. V. 73. P. 2532.

28. *Barrette J. et al.* // Phys. Rev. C. 1997. V. 56. P. 3254;
Barrette J. et al. // Phys. Rev. C. 1997. V. 55. P. 1420.

29. *Liu H. et al. (E895 collaboration)* // Nucl. Phys. A. 1998. V. 638. P. 451;
Liu H. et al. (E895 collaboration) // Phys. Rev. Lett. 2000. V. 84. P. 5488.

30. *Ogilvie C. et al.* // Nucl. Phys. A. 1998. V. 638. P. 57.

31. *Bannik B. et al.* // J. Phys. G. 1988. V. 14. P. 949.

32. *Adamovich M. et al.* // Eur. Phys. J. A. 1999. V. 6. P. 427.

33. *Simic Lj., Milosevic J.* // J. Phys. G. 2001. V. 27. P. 183.

34. *Keitz A. V. et al.* // Phys. Lett. B. 1991. V. 263. P. 353.

35. *Nishimura S. et al.* // Nucl. Phys. A. 1998. V. 638. P. 549.

36. *Aggarwal M. M. et al. (WA98 collaboration)*. e-print. Archive: nucl-ex/9807004. 1998.

37. *Appelshauser H. et al. (NA49 collaboration)* // Phys. Rev. Lett. 1998. V. 80. P. 4136.

38. *Ackermann K. et al.* // Phys. Rev. Lett. 2001. V. 86. P. 402.

39. *Danielewicz P., Odyniec D.* // Phys. Lett. B. 1985. V. 157. P. 146.

40. *Gyulassy M., Frankel K. A., Stöcker H.* // Phys. Lett. B. 1982. V. 110. P. 185;
Danielewicz P., Gyulassy M. // Phys. Lett. B. 1983. V. 129. P. 283.

41. *Ollitrault J.* // Phys. Rev. D. 1992. V. 46. P. 229;
Ollitrault J. // Phys. Rev. D. 1993. V. 48. P. 1132.

42. *Voloshin S., Zhang Y.* // Z. Phys. C. 1996. V. 70. P. 665;
Voloshin S. A. // Phys. Rev. C. 1997. V. 55. P. R1630;
Poskanzer A. M., Voloshin S. A. // Phys. Rev. C. 1998. V. 58. P. 1671.

43. *Buchward G. et al.* // Phys. Rev. C. 1983. V. 28. P. 2349.

44. *Csernai L. P.* Introduction Relativistic Heavy Ion Collisions. Singapore, 1994. P. 213.

45. *Ollitrault J.* nucl-ex/9711003. 1997;
Ollitrault J. // Nucl. Phys. A. 1998. V. 638. P. 195c.

46. *Nikonov E., Shanenko A., Toneev V.* // Heavy Ion Phys. 1998. V. 8. P. 89; nucl-th/9802018. 1998;
Nikonov E., Shanenko A., Toneev V. // Yad. Phys. 1999. V. 62. P. 1301.

47. *Rischke D. et al.* // Heavy Ion Phys. 1996. V. 1. P. 309;
Rischke D. // Nucl. Phys. A. 1997. V. 610. P. 88.

48. *Toneev V., Gudima K.* // Nucl. Phys. A. 1983. V. 400. P. 173.

49. *Chkhaidze L. et al.* // Phys. Lett. B. 1997. V. 411. P. 26.

50. *Beavis O. et al.* // Phys. Rev. C. 1992. V. 45. P. 299.

51. *Beavis O. et al.* // Phys. Rev. C. 1986. V. 33. P. 1113.

52. *Chkhaidze L. et al.* // Phys. Lett. B. 2000. V. 479. P. 21.

53. *Doss K. et al.* // Phys. Rev. Lett. 1987. V. 59. P. 2720.

54. *Gustafsson H. et al.* // Mod. Phys. Lett. A. 1980. V. 3. P. 1323.

55. *Gutbrod H., Poskanzer A., Ritter A.* // Rep. Prog. Phys. 1989. V. 52. P. 1267;
Harris J. et al. // Nucl. Phys. A. 1987. V. 471. P. 241c.

56. *Pinkenburg C. et al. (E895 collaboration)* // Phys. Rev. Lett. 1999. V. 83. P. 1295.

57. *Barrette J. et al.* e-print. Archive: nucl-ex/0007007. 2000;
Barrette J. et al. // Phys. Rev. C. 2001. V. 63. P. 014902.

58. *Justice M. et al.* // Nucl. Phys. A. 1995. V. 590. P. 549c;
Justice M. et al. e-print. Archive: nucl-ex/9708005. 1997;
Justice M. et al. // Phys. Lett. B. 1998. V. 440. P. 12.

59. *Barrette J. et al.* // Phys. Lett. B. 2000. V. 485. P. 319.

60. *Crochet Ph. et al. (FOPI collaboration)* // Nucl. Phys. A. 1996. V. 610. P. 49c.

61. *Balazs N. et al.* // Nucl. Phys. A. 1984. V. 424. P. 605.

62. *Lang A. et al.* // Z. Phys. A. 1991. V. 340. P. 287.

63. *Ajitanand N. N. et al.* // Nucl. Phys. A. 1998. V. 638. P. 451.

64. *Danielewicz P. et al.* // Phys. Rev. C. 1988. V. 38. P. 120.

65. *Gale C. et al.* // Phys. Rev. C. 1990. V. 41. P. 1545.

66. *Wong C. Y. et al.* // Phys. Rev. C. 1982. V. 25. P. 1460.

67. *Zhang S., Das Gupta S., Gale C.* // Phys. Rev. C. 1994. V. 50. P. 1617.

68. *Keane D. et al.* // Proc. of Nuclear Dynamics Workshop IV, Copper Mountain, Colorado, 1986 / Ed. by V. Viola. Springfield, 1986. P. 151; Report No. Conf-860270.

69. *Gosset K. et al.* // Phys. Rev. Lett. 1989. V. 62. P. 1251.

70. *Bass S. et al.* // Phys. Rev. C. 1995. V. 51. P. 3343.

71. *Kintner J. et al.* // Phys. Rev. Lett. 1997. V. 78. P. 4165.

72. *Li B. A., Bauer W., Bertch G.* // Phys. Rev. C. 1991. V. 44. P. 2095;
Li B. A. // Nucl. Phys. A. 1994. V. 570. P. 797.

73. *Li B. A., Ko C. M.* // Phys. Rev. C. 1995. V. 52. P. 2037;
Li B. A., Ko C. M. // Phys. Rev. C. 1996. V. 53. P. R22.

74. *Crochet Ph. et al.* // Phys. Lett. B. 2000. V. 486. P. 6.

75. *Chung P. et al.* // J. Phys. G. 1999. V. 25. P. 255.

76. *Kampert K. et al.* // J. Phys. G. 1989. V. 15. P. 691;
Gutbrod H. et al. // Rep. Prog. Phys. 1989. V. 52. P. 1261.

77. *Brill D. et al.* // Phys. Rev. Lett. 1993. V. 71. P. 336;
Brill D. et al. // Z. Phys. A. 1996. V. 355. P. 61.

78. *Venema L. et al.* // Phys. Rev. Lett. 1993. V. 71. P. 835.

79. *Pelte D. et al.* // Nucl. Phys. A. 1997. V. 622. P. 573.

80. *Hartnack C. et al.* // Phys. Lett. B. 1994. V. 336. P. 131.

81. *Danielewicz P. et al.* // Phys. Rev. Lett. 1998. V. 81. P. 2438;
Danielewicz P. et al. // Phys. Rev. C. 1995. V. 51. P. 716.

82. *Sorge H. et al.* // Phys. Rev. Lett. 1997. V. 78. P. 2309.

83. *Barrette J. et al.* // Nucl. Phys. A. 1995. V. 590. P. 259c.

84. *Li B. A., Ko C. M., Li G. Q.* // Phys. Rev. C. 1996. V. 55. P. 844.